THE JOURNAL OF PHYSICAL CHEMISTRY B

Article

pubs.acs.org/JPCB

Perrhenate Complexation by Uranyl in Traditional Solvents and in Ionic Liquids: A Joint Molecular Dynamics/Spectroscopic Study

Alain Chaumont,[†] Olga Klimchuk,[‡,§] Clotilde Gaillard,[∥] Isabelle Billard,*[,‡] Ali Ouadi,[‡] Christoph Hennig,[⊥] and Georges Wipff*[,†]

[†]Laboratoire MSM, UMR 7177, Institut de Chimie, 1 rue B. Pascal, 67000 Strasbourg, France

[‡]Institut Pluridisciplinaire Hubert Curien, DRS, Radiochimie, 23 rue du Lœss, 67037 Strasbourg cedex 2, France

[§]Institute of Organic Chemistry, NAS of Ukraine, 02660, Murmanska, 5, Kyiv, Ukraine

[∥]Université de Lyon, Institut de Physique Nucléaire de Lyon, CNRS-IN2P3, 4 rue Enrico Fermi, 69622 Villeurbanne cedex, France

[⊥]Institute of Radiochemistry, Forschungszentrum Dresden-Rossendorf, P.O. Box 510119, 01314 Dresden, Germany

Supporting Information

ABSTRACT: The complexation of perrhenate (ReO_4^-) anions by the uranyl (UO_2^{2+}) cation has been investigated by joint molecular dynamics simulations and spectroscopic (UV−vis, TRLFS, and EXAFS) studies in aqueous solution, acetonitrile, and three ionic liquids (ILs), namely, [Bmi][Tf_2N], [Me_3BuN][Tf_2N], and [Bu_3MeN]-[Tf_2N] that are based on the same Tf_2N^- anion (bis(trifluoromethylsulfonyl)-imide) and either Bmi^+ (1-butyl,3-methylimidazolium), Me_3BuN^+, or Bu_3MeN^+ cations. They show that ReO_4^- behaves as a weak ligand in aqueous solution and as a strong ligand in acetonitrile and in the ILs. According to MD simulations in aqueous solution, the $UO_2(ReO_4)_2$ complex quickly dissociates to form $UO_2(H_2O)_5^{2+}$, while in acetonitrile, a stable $UO_2(ReO_4)_5^{3-}$ species forms from dissociated ions. In the ILs, the $UO_2(ReO_4)_n^{2-n}$ complexes (n = 1 to 5) remained stable along the dynamics, and to assess their relative stabilities, we computed the free energy profiles for stepwise ReO_4^- complexation to uranyl. In the two studied ILs, complexation is favored, leading to the $UO_2(ReO_4)_5^{3-}$ species in [Bmi][Tf_2N] and to $UO_2(ReO_4)_4^{2-}$ in [Bu_3MeN][Tf_2N]. Furthermore, in both acetonitrile and [Bmi][Tf_2N] solutions, MD and PMF simulations support the formation of dimeric uranyl complexes $[UO_2(ReO_4)_4]_2^{4-}$ with two bridging ReO_4^- ligands. The simulation results are qualitatively consistent with spectroscopic observations in the different solvents, without firmly concluding, however, on the precise composition and structure of the complexes in the solutions.

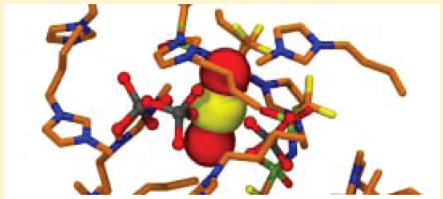

$UO_2(ReO_4)_3^-$ Complex in the [BMI]Tf_2N] Ionic Liquid

INTRODUCTION

Solvation strongly determines the coordination properties of uranyl, a cation of utmost importance in the context of nuclear plants and waste management.[1,2] The precise composition of its first coordination sphere in solution results from the competition between putative ligands (e.g., extractant molecules), different counterions, and solvent molecules, including water. Aqueous environments are indeed inherently involved in hydrometallurgy processes to concentrate uranyl or separate it from radioactive solutions or from polluted biological systems.[3] It is, however, important to also characterize the coordination chemistry in nonaqueous solvents where unusual coordination modes can be observed. See, for instance, the case of the $UO_2(NO_3)_3^-$ or $UO_2Cl_4^{2-}$ complexes unknown in water but characterized in acetonitrile or in ionic liquids.[4−6] Uranyl coordination to solvent molecules is also markedly solvent dependent. Intrinsically (i.e., in the gas phase), the $UO_2(MeCN)_5^{2+}$ complex is more stable than its aquo $UO_2(H_2O)_5^{2+}$ analogue, indicating that MeCN is a stronger ligand than water, as expected from the higher dipole moment and polarizability of MeCN, compared to those of H_2O.[7] In humid acetonitrile solution, however, uranyl prefers H_2O over MeCN ligands because $UO_2(H_2O)_5^{2+}$ interacts more strongly than $UO_2(MeCN)_5^{2+}$ with the surrounding medium.[7] Complexation with extractant molecules is also solvent dependent. For instance, 18-crown-6 forms an inclusion complex with uranyl triflate in acetonitrile but not in water.[8]

On an applied perspective, one of the problems to be tackled in nuclear fuel reprocessing is the concomitant extraction of uranium and technetium. The latter element has a long-lived β-emitting ^{99}Tc isotope ($t_{1/2} = 2 \times 10^5$ years) produced in high yield (ca. 6%) by uranium fission and is present after fuel dissolution in acidic water under its chemically most stable $Tc^{(VII)}$ form, i.e., the tetrahedral pertechnetate TcO_4^- ion. The presence of Tc in nuclear streams is deleterious because of its radiotoxicity and of its detrimental effect on the overall

Received: October 1, 2011
Revised: February 10, 2012
Published: February 13, 2012

   dx.doi.org/10.1021/jp209476h | J. Phys. Chem. B 2012, 116, 3205−3219

U/Pu separation.[9] In the PUREX process, TcO_4^- is extracted under various forms, in particular as mixed U−nitrate−pertechnetate complexes, requiring further steps (e.g., UREX + process) to separate Tc from the major actinides.[10,11] TcO_4^- has high mobility in the environment and is difficult to complex. It is thus important, from a practical and a fundamental perspective, to characterize its relationship with respect to uranyl (either a mere noncoordinated neutralizing counterion or an effective ligand) in different liquid environments.

For this purpose, we decided to use its nonradioactive chemical analogue, ReO_4^-. TcO_4^- and ReO_4^- have indeed similar bond distances (1.71 vs 1.72−1.73 Å), acido-basic properties (estimated pK_a = 0.03 vs −0.28) and coordination properties.[12] ReO_4^- has been used as a surrogate of TcO_4^- that is coextracted with uranyl by TBP (tri-*n*-butyl-phosphate) in the PUREX process, forming, e.g., $UO_2(NO_3)(TcO_4)(TBP)_2$ or $UO_2(TcO_4)_2(TBP)_2$ complexes.[13−15] There are X-ray structures of uranyl complexed with one[16] or two[17] TcO_4^- anions and phosphoryl containing ligands. There are also analogies between ReO_4^- and ClO_4^- that correspond to comparable strong acids.[18] The $UO_2(ClO_4)_2(H_2O)_6$ salt has been used as a source of uranyl to study its coordination by various anions (e.g., Cl^-),[19] assuming that ClO_4^- does not bind to uranyl, as suggested by EXAFS studies in water[20] and by a recent Car−Parrinello simulation study.[21] We thus want to investigate whether ReO_4^- anions can be complexed by UO_2^{2+} and what are the corresponding stoichiometries and structures in different solvents: water, acetonitrile, and three ionic liquids, [Bmi][Tf_2N], [Me_3BuN][Tf_2N], and [Bu_3MeN][Tf_2N]. The choice of these ILs is dictated by the potential these solvents present for liquid−liquid extraction of actinides, as recently reviewed.[22,23]

Following previous methodological approaches,[4,24,25] the systems are studied by molecular dynamics (MD) and spectroscopic (UV−vis, time-resolved laser induced fluorescence spectroscopy TRLFS, and extended X-ray absorption fine structure EXAFS) studies on similar systems, and by quantum mechanical (QM) calculations to gain insights into the intrinsic (gas phase) complexation of ReO_4^- by uranyl. Solution studies are made first in classical liquids, where uranyl has been extensively studied, namely, water and acetonitrile, and then in hydrophobic room temperature ionic liquids (ILs) that represent recently developed fascinating media where actinide cations can be extracted by classical complexing molecules[22,26,27] or solubilized.[28,29] For this purpose, we compare the [Bmi][Tf_2N] to the [Bu_3MeN][Tf_2N] and [Me_3BuN][Tf_2N] ILs that are based on the same Tf_2N^- anion (bis(trifluoromethylsulfonyl)imide $(CF_3SO_2)_2N^-$) and either Bmi^+ (1-butyl,3-methylimidazolium), Bu_3MeN^+ (tributylmethylammonium), or Me_3BuN^+ (trimethylbutylammonium) cations. These IL components have been used to study uranyl speciation in the presence of various anions (PF_6^-, Tf_2N^-, Cl^-, F^-, BF_4^-, and NO_3^-).[4,5,24,30]

SIMULATION METHODS

Molecular Dynamics. The different systems were simulated by classical molecular dynamics using the modified PMEMD version of the AMBER10 software[31] in which the potential energy U is described by a sum of bond, angle, and dihedral deformation energies and pairwise additive 1−6−12 (electrostatic and van der Waals) interactions between nonbonded atoms as follows:

$$U = \sum_{\text{bonds}} k_b(r - r_0)^2 + \sum_{\text{angles}} k_\theta(\theta - \theta_0)^2 + \sum_{\text{dihedrals}} \sum_{n} V_n(1 + \cos(n\varphi - \gamma)) + \sum_{i<j} \left[\frac{q_i q_j}{R_{ij}} - 2\varepsilon_{ij}\left(\frac{R_{ij}^*}{R_{ij}}\right)^6 + \varepsilon_{ij}\left(\frac{R_{ij}^*}{R_{ij}}\right)^{12} \right] \quad (1)$$

Cross-terms in van der Waals interactions were constructed using the Lorentz−Berthelot rules. Force field parameters for the pure ionic liquid were taken from ref 32 for Bmi^+, and ref 33 for Tf_2N^-. These parameters have been shown to give good agreement with experimental data for the neat liquids.

The parameters of UO_2^{2+} and ReO_4^- are from refs 34 and 35, respectively. The charges of ReO_4^- (q_{Re} = 1.436 e; q_O = −0.609 e) were fitted on ESP electrostatic potentials obtained at the HF/cc-pVTZ level. A summary of the force field parameters of ReO_4^- is given in Figure S1, Supporting Information. The 1−4 van der Waals and 1−4 Coulombic interactions were scaled down by 2.0, as recommended by Sieffert et al.[36] The solutions were simulated with 3D-periodic boundary conditions. Nonbonded interactions were calculated using a 12 Å atom based cutoff, calculating the long-range electrostatics by using the Ewald summation method in the Particle Mesh Ewald (PME) approximation.

The MD simulations were performed at 300 K for water and acetonitrile solutions, and at 400 K for the IL solutions to enhance the sampling. They started with random velocities, using the Verlet leapfrog algorithm with a time step of 1 fs to integrate the equations of motion. The temperature was monitored by coupling the system to a thermal bath using the Berendsen algorithm with a relaxation time of 0.2 ps. All C−H bonds were constrained using the Shake algorithm.

For the IL solutions, we first equilibrated cubic boxes of pure liquids of about 40 Å lengths, containing about 200 pairs of Bmi^+ Tf_2N^- or Bu_3MeN^+ Tf_2N^- ions. We then immersed the different complexes $(UO_2(ReO_4)_n^{2-n}$, n = 0−6) in the box. To keep the same number of solute species in the different systems and to maintain neutrality, we added $6 - n$ free ReO_4^- anions (placed at ca. 15 Å from the U atom) and removed 4 Tf_2N^- IL ions. The characteristics of the simulated classical (water and acetonitrile) and IL solutions are summarized in Table S1, Supporting Information.

Equilibration started with 2000 steps of steepest descend energy minimization, followed by 0.25 ns with fixed solutes (BELLY option in AMBER) at constant volume, by 0.25 ns of constant volume without constraints, and by 0.5 ns at a constant pressure of 1 atm coupling the system to a barostat with a relaxation time of 0.2 ps. This was followed by 5 ns of MD in the (NVT) ensemble at 300 K for the aqueous and acetonitrile solutions or at 400 K for the IL solutions. Because of the high viscosity of ILs and related slow diffusion processes, we next repeated 4 times the following sequence to enhance the sampling: (i) heating to 500 K for 1 ns with reduced Coulombic interactions (divided by a factor 1000); (ii) relaxation for 0.5 ns at 400 K with reset electrostatics. At stages (i) and (ii), the solutes were fixed (BELLY option in AMBER) to avoid dissociation of the complex. (iii) This was

dx.doi.org/10.1021/jp209476h | J. Phys. Chem. B 2012, 116, 3205−3219

followed by a MD run of 5 ns at constant volume at 400 K without constraints. For every IL solution, we thus run 5 MD runs of 5 ns each.

The MD trajectories were saved every 1 ps and analyzed with the MDS and DRAW software[37] and typical snapshots were redrawn using VMD.[38] The average structure of the solvent around UO_2^{2+} was characterized by the radial distribution functions (RDFs) of the anions and cations. The average coordination number (CN) of the solvent anions (O and N atoms of Tf_2N^-) and cations (N_{butyl} atom of Bmi^+ or N atom of Bu_3MeN^+) were calculated by integration of the first peak of the RDF. Insights into energy features were obtained by group component analysis, using a 12 Å cutoff and PME Ewald correction of long range electrostatics. Averages were calculated over the last 1 ns of each MD run (total 5 ns).

Free Energy Calculations. The free energy profiles for ReO_4^- anion complexation were calculated as a function of the U···Re distance d (Potential of mean force, PMF, calculations).[39,40] The complexation reactions started with the uncomplexed ReO_4^- anion found at the shortest distance from uranyl after the 5 × 5 ns of dynamics (see Simulation Methods sections), i.e., at d ca. 12 to 18 Å (initial state; $\lambda = 1$). They were conducted by small steps ($\Delta d = 0.01$ Å) until the anion was coordinated to uranyl, i.e., at ca. 3.0 Å (final state; $\lambda = 0$). The change in free energy was calculated at each λ step using the TI method and cumulated from $\lambda = 0$ to 1 (see eq 2 and details for each system in Table S2, Supporting Information).

$$\Delta G = \int_0^1 \left\langle \frac{\partial U}{\partial \lambda} \right\rangle_\lambda \mathrm{d}\lambda \qquad (2)$$

At each λ step, we performed 10 ps of equilibration followed by 40 ps of data collection. The corresponding free energy of complexation ΔG_c was calculated as the difference between ΔG at the first minimum or plateau (uncomplexed ReO_4^-, at d = ca. 15 Å to 12 Å, depending on the system) and ΔG at the energy minimum (complexed ReO_4^-, at $d \approx 2.5$ Å).

Quantum Mechanical (QM) Calculations. The different uranyl complexes were optimized with the Gaussian03 software[41] at the HF and DFT (B3LYP) levels of theory. For U and Re atoms, we used the small-core Stuttgart–Dresden (SDD) relativistic effective core potential (ECP) together with their valence basis sets.[42] For the U atom, each most diffuse s-, p-, d-, and f-function was omitted, affording a [7s6p5d3f] contraction. The O, S, C, F, and N atoms were represented with the cc-pvTZ basis set.[43] The minimum energy character of each stationary point was verified by computation of the harmonic vibrational frequencies that were all found to be real.

EXPERIMENTAL SECTION

Chemicals. Ag_2O, $AgNO_3$, $HClO_4$ (70 wt % solution in water), $HReO_4$ (VWR, 65 − 70% solution in water), Me_2BuN, and $Bu_3MeN{\cdot}OH$ (Aldrich, 20 wt % solution in water) were used as received. The synthesis of $UO_2(Tf_2N)_2$ has been published elsewhere.[6] This yellowish salt is highly hygroscopic, so that, for all experiments, great care has been taken to dry it thoroughly on a vacuum line prior to use. $[Bu_3MeN][Tf_2N]$ (99.9%), $[Me_3BuN][Tf_2N]$ (99.5%), and $[Bmi][Tf_2N]$ (99.5%) have been purchased from Solvionic (Toulouse, France).

1-Butyl-3-methylimidazolium Perrhenate $BmiReO_4$. Solid silver(I) perrhenate (5.0 g, 13.96 mmol) was added to a solution of 1-butyl-3-methylimidazolium bromide (BmiBr) (2.90 g, 13.26 mmol) in deionized water (30 mL), and the suspension was stirred in the dark at rt for 12 h. The precipitated AgBr was filtered off and the water was evaporated. The crude $BmiReO_4$ was dissolved in CH_2Cl_2, precipitated crystals were filtered off, and the filtrate was evaporated. The product was dried at 70 °C in vacuo for 24 h and was obtained as a viscous colorless oil (5.0 g, 96.3% yield).

^{1}H NMR (300 MHz, D_2O) δ: 0.65 (t, 3H, $NCH_2CH_2CH_2CH_3$), 1.11 (m, 2H, $NCH_2CH_2CH_2CH_2$), 1.75 (q, 2H, $NCH_2CH_2CH_2$), 3.68 (s, 3H NCH_3), 3.97 (t, NCH_2), 7.20 (d, 2H, NCHCHN), 8.45 (s, 1H, NCHN). ^{13}C NMR (300 MHz, D_2O) δ: 12.62, 18.76, 31.27, 35.59, 49.29, 122.21, 123.47, 135.80. HRMS (ESI) m/z (%): calcd for $C_8H_{15}N_2O_4Re$ (M^+), 139.126; found, 139.130; (M^-) 250.25; found, 250.210.

Tributylmethylammonium Perrhenate $Bu_3MeNReO_4$. To a solution of tributylmethylammonium hydroxide (10.85 g, 10 mmol) in water, a solution of perrhenic acid (3.86 g, 10 mmol) was added, and the solution was stirred at rt for 6 h. The precipitated $Bu_3MeNReO_4$ was filtered and was dried at 70 °C in vacuo for 12 h. Product was obtained as colorless crystals (3.7 g, 82.2%).

^{1}H NMR (300 MHz, $CDCl_3$) δ: 1.05 (t, 9H, $NCH_2CH_2CH_2CH_3$), 1.46 (m, 6H, $NCH_2CH_2CH_2CH_2$), 1.64 (m, 6H, $NCH_2CH_2CH_2$), 3.05 (s, 3H NCH_3), 3.27 (m, 6H, NCH_2). ^{13}C NMR (300 MHz, $CDCl_3$) δ: 13.62, 19.73, 24.26, 48.35, 61.86. HRMS (ESI) m/z (%): calcd for $C_{13}H_{30}NO_4Re$, (M^+) 200.237; found, 200.39; (M^-) 250.933; found, 250.210.

Trimethylbutylammonium Perrhenate $Me_3BuNReO_4$. The suspension of trimethylbutylammonium iodide (2.43 g, 10 mmol) in deionized water (17 mL) and silver(I) oxide (1.16 g, 5 mmol) was stirred in the dark at rt for 12 h. The precipitated AgI was filtered off, and the resulting Me_3BuNOH solution was isolated after titration for the next step.

To a solution of Me_3BuNOH (3.3 mL), perrhenic acid was added (0.48 g, 1.80 mmol, 65% solution in water), and the resulting solution was stirred at rt for 6 h. Water was evaporated. The product was purified by crystallization from EtOH. $Me_3BuNReO_4$ was dried at 70 °C in vacuo for 12 h and was obtained as colorless crystals (0.52 g, 77.1 yield %).

^{1}H NMR (300 MHz, D_2O) δ: 0.65 (t, 3H, $NCH_2CH_2CH_2CH_3$), 1.15 (m, 2H, $NCH_2CH_2CH_2CH_2$), 1.51 (m, 2H, $NCH_2CH_2CH_2$), 2.82 (s, 9H NCH_3), 3.07 (m, 2H, NCH_2). ^{13}C NMR (300 MHz, D_2O) δ: 12.78, 19.05, 24.28, 52.68, 52.73, 52.79, 66.55. HRMS (ESI) m/z (%): calcd for $C_7H_{18}NO_4Re$ (M^+), 116.143; found, 116.194; (M^-) 250.933; found, 250.210.

Solutions. For all the samples of this work, uranyl was added via the $UO_2(Tf_2N)_2$ salt. Aqueous solutions have been prepared with ultra pure Milli-Q water. Depending on the type of measurements (TRLFS or UV–vis), the uranyl concentration was either 10^{-3} M (TRLFS) or 10^{-2} M (UV–vis). Two series of aqueous solutions were prepared:

(i) First series: $HReO_4$ concentration was varied from 10^{-2} M to 6.22 M; $[UO_2^{2+}] = 10^{-2}$ M.
(ii) Second series: $HReO_4$ concentration was varied from 10^{-2} M to 6.38 M; $[UO_2^{2+}] = 10^{-3}$ M.

Therefore, in water, the ratio $R = [ReO_4^-]/[UO_2^{2+}]$ varied from 1 to 620 (first series, UV–vis) and from 10 to 6400 (second series, TRLFS). In acetonitrile (dried over phosphorus pentoxide and calcium hydride), R has been varied either by the addition of $BmiReO_4$ (ratio from 0 to 5) or $Bu_3MeNReO_4$ (ratio equal to 10 and 20). Uranyl concentration was equal to 10^{-2} M. ILs solutions were prepared by dissolving the requested amount of uranyl (10^{-2} M) and perrhenate salts in

dx.doi.org/10.1021/jp209476h | J. Phys. Chem. B 2012, 116, 3205–3219

5 mL of IL solvent. The perrhenate salt ($BmiReO_4$, $Me_3BuNReO_4$, or $Bu_3MeNReO_4$) was chosen in accordance to the cationic component of the IL under study for consistency. The resulting solutions were thereafter carefully degassed according to previously published procedure.[44] In addition, to shield samples from light, these were carefully wrapped in Al foil and kept in the dark in between experiments. Without this precaution, precipitation, as a yellowish-greenish flaky powder, occurred in all of the solutions within a few days of day light exposure. We did not attempt to identify the nature of the precipitate, but its occurrence has been clearly ascribed to light exposure (as samples kept in dark displayed no precipitate even after several weeks) and to the simultaneous presence of uranyl and rhenium. All data presented in this work for the IL samples correspond to spectra recorded at least 2 days after sample preparation, a delay long enough to check for their stability.

Measurements. The aqueous acidic solutions have been titrated with an automatic titrator to check the exact $[H^+]$ values (Schott, titroline). Uncertainties in the $[H^+]$ determination were within 2%.

For all the IL solutions, the remaining water content has been checked by IR (Bruker, Equinox 55, quartz cuvette, 1 cm pathway) at the end of the measurements, by comparison with the IR spectra of the three pure ILs before and after degassing. In agreement with previous works,[45,46] the water peak is present in the 5200−5350 cm^{-1} range for the three ILs. For the degassed samples, no significant amount of water could be detected. Figure S2, Supporting Information, displays the IR spectra in the 6500−5000 cm^{-1} range for the three degassed ILs, showing the various patterns ascribed to the cations.

UV−vis absorption spectroscopy was performed on a Varian, Uvikon 100, with quartz cuvettes of 1 cm path way, in the range 200−800 nm. The temperature was controlled at $T = (18 \pm 0.5)$ °C. Previous trials have shown that the Teflon caps are tight enough to prevent water from entering the IL samples, even for a long period of time (up to months).[45] UV−visible absorption spectra were recorded taking either pure acetonitrile or the corresponding pure degassed ILs as a reference for samples in acetonitrile or in ILs, respectively. For the pure ILs samples, an empty quartz cuvette was used as a reference. Finally, for the aqueous samples with increasing $HReO_4$ concentrations, the reference was $HReO_4/H_2O$ solutions of increasing concentrations, accordingly.

Time-resolved laser induced fluorescence spectroscopy (TRLFS) was performed with a setup described elsewhere.[30] Temperature was controlled at $T = (21 \pm 0.5)$ °C. In this work, laser excitation was set at $\lambda = 355$ nm instead of $\lambda = 266$ nm, owing to the large absorption coefficient of ReO_4^- in the far UV range, which therefore would have prevented any uranyl luminescence detection. As our setup is not calibrated for energy compensations, the relative intensities are of no physical meaning, by contrast to the peak positions. Data are thus presented as emission features in the range 470−580 nm (uncertainties on the emission peak position: ± 0.5 nm).

EXAFS Data Analysis. Samples were prepared with the same protocol as explained above, one week before the experiment during which they were kept in the dark. EXAFS measurements were led at the ROBL-ESRF beamline, at ambient temperature, using a double crystal Si(111) monochromator. Analysis were made at the U L_{III} (17166 eV) edge in transmission mode using argon-filled ionization chambers and for one sample also at the Re L_{III} edge (10535 eV) in fluorescence mode. The monochromator energy was calibrated by an yttrium foil (17038 eV) for the U edge and a Zn foil (9659 eV) for the Re edge. XAFS data reduction was made using the IFEFFIT code.[47] Data analysis was carried out with the FEFFIT code,[48] using phase and backscattering amplitude functions generated with the FEFF 8.1 code.[49] Fits of the Fourier transform (FT) k^3-weighted EXAFS data to the EXAFS equation were performed in R-space between 1 and 4.3 Å for U L_{III} spectra and between 0.6 and 4.5 Å for the Re L_{III} spectrum. The k-range used was 3.0−16.8 $Å^{-1}$ for U L_{III} spectra and 2.6−16.1 $Å^{-1}$ for the Re L_{III} spectrum. The amplitude reduction factor (S_0^2) was held constant to 1 for all fits. The shift in the threshold energy (E_0) was allowed to vary as a global parameter for all atoms. In all U L_{III} spectra fits, the coordination number of the uranyl axial oxygen atoms (O_{ax}) was held constant at two. The multiple scattering paths of the axial oxygens were included in the curve fit by constraining its effective path-length to twice the values of the corresponding U−O_{ax} distance.

SIMULATION RESULTS

In this section, we present simulation results on the binding strength of ReO_4^- to uranyl in the gas phase (QM studies) and in water, acetonitrile, and ionic liquids solutions (studied by MD and PMF). The choice of simulated solutions was inspired by the experimentally studied ones, using sometimes somewhat different conditions, due to computer time limitations. The MD studies afford valuable insights into the coordination properties of ReO_4^- to uranyl in the different solvents.

Gas Phase. Using QM (HF and DFT/B3LYP) and molecular mechanics (MM) methods, we have optimized the $UO_2(ReO_4)_n^{2-n}$ (n = 1−6) complexes as well as $UO_2(Tf_2N)(ReO_4)_4^{3-}$ in the gas phase where all ligands remain coordinated in the equatorial plane of UO_2^{2+}. In the $UO_2(ReO_4)_n^{2-n}$ series, ReO_4^- ligands evolve from bidentate to monodentate coordination when n increases: in the unsaturated $UO_2(ReO_4)^+$ and $UO_2(ReO_4)_2$ complexes, they are bidentate, whereas in the saturated $UO_2(ReO_4)_5^{3-}$ and $UO_2(ReO_4)_6^{4-}$ complexes, they are monodentate. In the intermediate $UO_2(ReO_4)_3^-$ and $UO_2(ReO_4)_4^{2-}$ complexes, there is a mix of coordination modes (2 bi- and 1 monodentate for the former; 3 mono- and 1 bidentate for the latter). U−Re distances are in the range of 3.2−3.5 Å in the case of bidentate coordinating ReO_4^- anions, while for monodentate coordinating ReO_4^- anions, distance are somewhat longer (4.1−4.3 Å) (Table S3, Supporting Information). As expected, U−Re distances increase with the number of coordinated ReO_4^- anions.

$$UO_2(ReO_4)_n^{2-n} + ReO_4^- \rightarrow UO_2(ReO_4)_{n+1}^{1-n} \quad (3)$$

The HF and DFT energies of stepwise complexation reactions of ReO_4^- (eq 1; see Table 1) indicate that complexation is favored for the first three anions but not for the next ones. Thus, in the gas phase, uranyl coordinates at most 3 (bidentate) ReO_4^- anions, as found for Cl^- or SCN^- analogues,[50,51] due to steric and Coulombic repulsions between the negatively charged $UO_2(ReO_4)_3^-$ complex and an additional ReO_4^- ligand.[52]

In the presence of IL anions, uranyl can coordinate O_{Tf2N} as well as O_{ReO4} oxygens. To study the ReO_4^-/Tf_2N^- competition with a 5-coordination, we considered reaction 7 in Table 1, showing that at the HF and DFT levels of theory, uranyl slightly prefers ReO_4^- over Tf_2N^- (by ca. 3 kcal/mol) and that

dx.doi.org/10.1021/jp209476h | J. Phys. Chem. B 2012, 116, 3205−3219

Table 1. Complexation Energies (in kcal/mol) of ReO_4^- in the Gas Phase

	reaction	HF	B3LYP	MM
(1)	$UO_2^{2+} + ReO_4^- \rightarrow UO_2(ReO_4)^+$	−281.2	−302.9	−215.1
(2)	$UO_2(ReO_4)^+ + ReO_4^- \rightarrow UO_2(ReO_4)_2$	−153.8	−154.6	−156.3
(3)	$UO_2(ReO_4)_2 + ReO_4^- \rightarrow UO_2(ReO_4)_3^-$	−55.7	−53.4	−61.3
(4)	$UO_2(ReO_4)_3^- + ReO_4^- \rightarrow UO_2(ReO_4)_4^{2-}$	8.1	12.0	3.7
(5)	$UO_2(ReO_4)_4^{2-} + ReO_4^- \rightarrow UO_2(ReO_4)_5^{3-}$	65.3	68.7	55.3
(6)	$UO_2(ReO_4)_5^{3-} + ReO_4^- \rightarrow UO_2(ReO_4)_6^{4-}$	143.4	141.0	116.2
(7)	$UO_2(ReO_4)_4(Tf_2N)^{3-} + ReO_4^- \rightarrow UO_2(ReO_4)_5^{3-} + Tf_2N^-$	−3.5	−3.2	−17.7
(8)	$UO_2(Tf_2N)_2 + 2\ ReO_4^- \rightarrow UO_2(ReO_4)_2 + 2\ Tf_2N^-$	3.0	0.3	1.8

this feature is also accounted for with the FF calculation. However, in unsaturated 4-coordinated UO_2X_2 neutral complexes, the trend is inversed, i.e., Tf_2N^- is slightly preferred (see reaction 8 in Table 1).[53] Thus, the result of the Tf_2N^- vs ReO_4^- competition depends on the extra ligands (including solvent molecules) that contribute to the saturation of the first coordination shell and modulate the binding mode of Tf_2N^- (from mono- to polydentate).

Aqueous Solution. We first simulated the $UO_2(ReO_4)_2$ neutral complex in aqueous solution. In this dissociating medium, the complex proved to be unstable and quickly dissociated to form the hydrated UO_2^{2+} and 2 ReO_4^- species. In the course of the dynamics (20 ns), these ions remain dissociated, apart from a few exceptions where one ReO_4^- anion binds to UO_2^{2+} to form $UO_2ReO_4(H_2O)^+$, of short lifetime, though (ca. 100–200 ps; see Figure 1). Increasing the Re/U ratio also increases

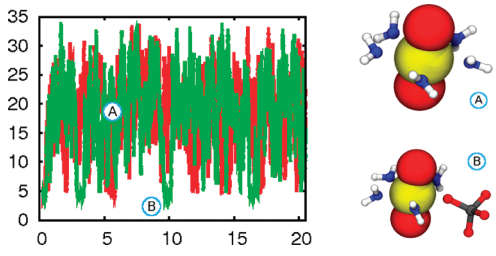

Figure 1. $UO_2(ReO_4)_2$ simulated in water: Re_x–U distances (Å) as a function of time (ns) (left). Typical snapshots along the trajectory (right).

the lifetime of complexed ReO_4^- and the degree of complexation in water, as seen by simulations of solutions containing one uranyl and either 75 H_3O^+ ReO_4^- or 125 H_3O^+ ReO_4^- ion pairs, yielding average coordination numbers of 1.3 ± 1.1 and of 2.1 ± 1.2, respectively, over 20 ns. Coordination in water is highly dynamic and fluctuating, involving exchanges from zero- to penta-complexed forms, of rather short lifetimes (Figure 2). The complexes can thus be hardly depicted by a single dominant species.

Acetonitrile Solution. In acetonitrile, we investigated the competition between ReO_4^- and Tf_2N^- uranyl ligands in the presence of Bmi^+ or Bu_3MeN^+ cations that are the components of the studied ILs. For this purpose, a preformed $UO_2(Tf_2N)_2$ complex was first immersed in an acetonitrile solution containing 5 Bmi^+ and 5 ReO_4^- uncomplexed ions. During the dynamics, uranyl lost its two Tf_2N^- ligands (after 31.3 and 46.8 ns) and finally captured the five ReO_4^- anions (after 0.1 ns, 14.8 ns, 14.9 ns, 46.0 ns, and 72.9 ns, respectively) to form $UO_2(ReO_4)_5^{3-}$. The complexes formed along the dynamics are shown in Figure S3, Supporting Information (see also the evolution of U–Re distances in Figure S4, Supporting Information). Furthermore, when a $UO_2(ReO_4)_5^{3-}$ complex was simulated in an acetonitrile solution containing 2 Tf_2N^- and 5 Bmi^+ ions, it remained unchanged during the whole dynamics (100 ns), supporting its thermodynamic and kinetic stability (Figure S4, Supporting Information). This complex is surrounded on the average by 3.0 Bmi^+ cations at $U–N_{butyl}$ distances of about 9 Å, leading to an overall neutral aggregate.

To investigate whether the nature of the IL cations influences the stability of this $UO_2(ReO_4)_5^{3-}$ complex, we replaced Bmi^+ by Bu_3MeN^+ counterions in the simulation of the $UO_2(Tf_2N)_2$ salt: as above, in the course of the dynamics, the latter gradually dissociated and evolved to $UO_2(ReO_4)_5^{3-}$, confirming that monomeric uranyl can bind up to 5 ReO_4^- anions in this classical medium (Figure S4, Supporting Information).

The above simulations dealt with a single uranyl per solvent box, corresponding to a concentration of ca. 0.02 mol/L. To gain insights into concentration effects, we decided to simulate a similar system, but ca. three times more concentrated, thus containing initially 3 $UO_2(Tf_2N)_2$ complexes, plus 15 ReO_4^- Bmi^+ ions randomly distributed in the acetonitrile box. Progressively, along the dynamics, ReO_4^- displaced Tf_2N^- ligands, as above. However, after ca. 55 ns, an interesting feature appeared, namely, the formation of a uranyl dimer of $(UO_2)_2(ReO_4)_8^{4-}$ composition, involving two bridging ReO_4^- anions, plus 3 ReO_4^- exo ligands per uranyl (see Figure 3). This dimer remained stable until the end of the dynamics (250 ns; see U···U distances in Figure S5 and U–Re distances in Figure S6, Supporting Information). Furthermore, it underwent an interesting fluxional ligand exchange process from one uranyl to the other, via a bridging position: after ca. 81 ns, a ReO_4^- free anion diffused from the bulk (at ca. 25 Å from the dimer; blue

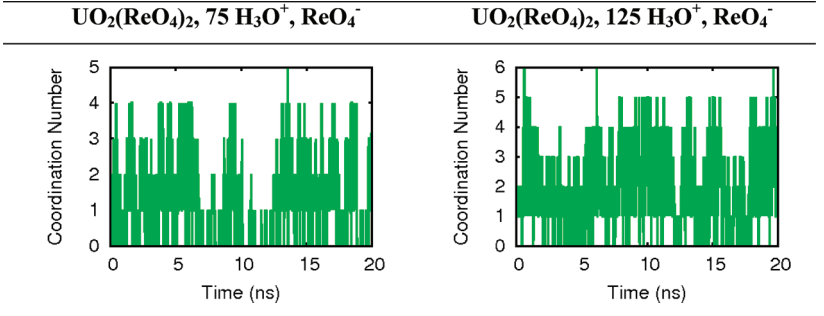

Figure 2. Simulation of $UO_2(ReO_4)_2$ in water in the presence of an excess of ReO_4^- ions (either 75 H_3O^+, ReO_4^- or 125 H_3O^+, ReO_4^-): number of ReO_4^- coordinated to uranyle is seen as a function of time.

dx.doi.org/10.1021/jp209476h | J. Phys. Chem. B 2012, 116, 3205–3219

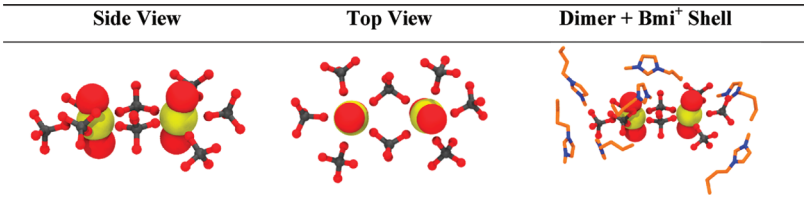

Figure 3. Snapshots of the uranyl dimer $(UO_2)_2(ReO_4)_8^{4-}$ formed in acetonitrile with its neutralizing Bmi^+ shell.

colored in Figure S7, Supporting Information) toward the dimer and coordinated as an extra exo ligand, forming the $(UO_2)_2(ReO_4)_9^{5-}$ complex. About 64 ns later, it moved to a bridging position and, ca. 36 ns later, moved as the exo ligand of the second uranyl. Finally, one ReO_4^- decomplexed to form again the $(UO_2)_2(ReO_4)_8^{4-}$ dimer.

Ionic Liquid Solutions. We have studied the solvation and stability of different $UO_2(ReO_4)_n^{2-n}$ (n = 0−6) complexes in the [Bmi][Tf_2N] and [Bu_3MeN][Tf_2N] ionic liquids. Solvent RDFs and typical snapshots of the solvation around the complexes are given in Figures 4 and S8, Supporting Information. During the dynamics, all complexes remained stable, except $UO_2(ReO_4)_6^{4-}$, which lost one ligand to form $UO_2(ReO_4)_5^{3-}$. In the different complexes, all ReO_4^- ligands coordinate monodentate to the U atom, at average U−O_{ReO4} distances of 2.40 Å. The solvation of the different complexes in both liquids depends on their charge: it evolves from purely anionic around UO_2^{2+} (4 to 5 Tf_2N^- species; see also ref 4) to purely cationic around $UO_2(ReO_4)_5^{3-}$. Interestingly, the number of Tf_2N^- anions coordinated to uranyl is slightly higher in the Bmi^+ than in the Bu_3MeN^+ based IL (Table 2): 5.0 vs 4.3 for UO_2^{2+}, 4.1 vs 4.0 for $UO_2ReO_4^+$, 3.5 vs 3.0 for $UO_2(ReO_4)_2$, 2.1 vs 2.0 $UO_2(ReO_4)_3^-$, and 1.5 vs 1.0 for $UO_2(ReO_4)_4^{2-}$. Taking into account the coordinated IL anions, one sees that uranyl forms anionic complexes of ca. −2.5 to −3.5 e charge. These are surrounded by IL cations (12−13 Bmi^+ or 9−11 Bu_3MeN^+ within 11−12 Å from the U atom), leading to the onion type solvation patterns with charge alternation as reported earlier.[50,54−56] Comparing the two ILs, we note that the cationic charge density around a given complex is thus somewhat higher in the [Bmi][Tf_2N] than in the [Bu_3MeN][Tf_2N] ionic liquid. Furthermore, looking at the solvation of ReO_4^- and Tf_2N^- ligands by the IL cations, one sees that Bmi^+ can form H-bonds via its C_2H imidazolium ring proton, whereas the quaternary ammonium Bu_3MeN^+ cannot, suggesting that the former displays stronger attractions with the anionic uranyl complex, as supported by the following energy component analysis.

To gain insights into energetics of the complexes in solution, we dissected the total energy E_{TOT} of the system into three components: E_{COMP} (intracomplex energy) + E_{SOLV} (interaction energy between the complex and the solvent) + E_{ILIL} (intrasolvent energy, including noncoordinated ReO_4^- anions as part of the solvent). Results are reported in Table 3. The E_{COMP} energies are negative (from ca. −180 to −380 kcal/mol) and of comparable magnitude in the two ILs for a given $UO_2(ReO_4)_n^{2-n}$ complex. Furthermore, when comparing a complex (n) to the next one (n + 1), one sees that E_{COMP} becomes more negative until four ReO_4^- anions are complexed. Adding a fifth anion destabilizes E_{COMP}, indicating that this component alone favors a 4-coordinated complex.[57]

The solvation energies E_{SOLV} are all negative (−220 to −580 kcal/mol) and of the highest magnitude for the most charged complexes, as expected from the simple Born solvation model.[58] Furthermore, a given complex is generally better solvated in the [Bmi][Tf_2N] than in the [Bu_3MeN][Tf_2N] IL (by 30−40 kcal/mol), supporting stronger interaction of ReO_4^- ligands with Bmi^+ than with Bu_3MeN^+ cations, as suggested above. The internal energy E_{ILIL} of the IL itself also varies, by up to 300 kcal/mol, depending on the state of the solute, and is often antagonistic to changes of the E_{COMP} and E_{SOLV} energies. As a result, the total energies E_{TOT} of the different systems are fairly constant within statistical fluctuations (ca. ± 70 kcal/mol) in a given IL and do not thus allow us to conclude about the relative stabilities of the different complexes. This is why we have undertaken PMF simulations in the IL solution (see next section).

Free Energy Profiles for Monomeric and Dimeric Complexes in IL Solution. The free energy profiles of the successive complexation of up to 5 ReO_4^- species by uranyl were obtained by PMF calculations in the [Bmi][Tf_2N] and [Bu_3Me N][Tf_2N] ionic liquids. They are shown in Figure 5, and the resulting complexation free energies ΔG_c are reported in Table S2, Supporting Information. The PMF curves show that, as the three first ReO_4^- anions approach from ca. 12 Å to 6−7 Å from uranyl, ΔG increases by ca. 4 to 6 kcal/mol in both ILs and then drops to a minimum of ca. −4 to −8 kcal/mol corresponding to the complexed anion. For the fourth and fifth ReO_4^- anions, PMF results are IL dependent and less clear-cut but indicate lower coordination of ReO_4^- by uranyl in the [Bu_3MeN][Tf_2N] than in the [Bmi][Tf_2N] IL. Indeed, in [Bmi][Tf_2N], the five complexation steps are clearly exergonic (by −6.9, −6.0, −7.9, −5.5, and −8.1 kcal/mol, respectively), i.e., favorable. In [Bu_3MeN][Tf_2N], complexation is exergonic for the three first anions only (−4.7, −9.9, and −6.8 kcal/mol, respectively) but of nearly zero and positive energies (−0.3 and 5.6 kcal/mol) for the subsequent additions, indicating that uranyl binds at most four ReO_4^- anions in this solvent. Thus, as found for SCN^- complexation to trivalent lanthanides,[51] the number of complexed ReO_4^- ligands can be modulated by the IL cation: it is higher with Bmi^+ than with Bu_3MeN^+ cations because the former afford H-bonding interactions with the anionic uranyl complex and a higher cationic charge density in its first solvation shell.

The complexes simulated so far are monomeric, corresponding to diluted solutions. However, as observed here (vide supra) for the simulated acetonitrile solutions (see also the X-ray structure of dimeric complexes $[UO_2(\mu_2\text{-}ReO_4)(ReO_4)L_2]_2$ with phosphorylated ligands L[42,59]), formation of uranyl oligomers cannot be precluded in the ILs. This led us to simulate IL solutions with two $UO_2(ReO_4)_4^{2-}$ complexes, where no dimer formed, even after 5 ns of MD at 400 K, presumably because diffusion is too slow. We thus decided to calculate the free energy profile for uranyl dimerization in the [Bmi][Tf_2N] IL, with a Re/U ratio of 4 as in experiments (see below), starting from two $UO_2(ReO_4)_4^{2-}$ complexes at a U···U distance d of 19.1 Å. The results (Figure 6a) show that as the anionic complexes approach each other, the free energy first increases, up to a maximum of ca. 8 kcal/mol at d = 8.3 Å and then

dx.doi.org/10.1021/jp209476h | J. Phys. Chem. B 2012, 116, 3205−3219

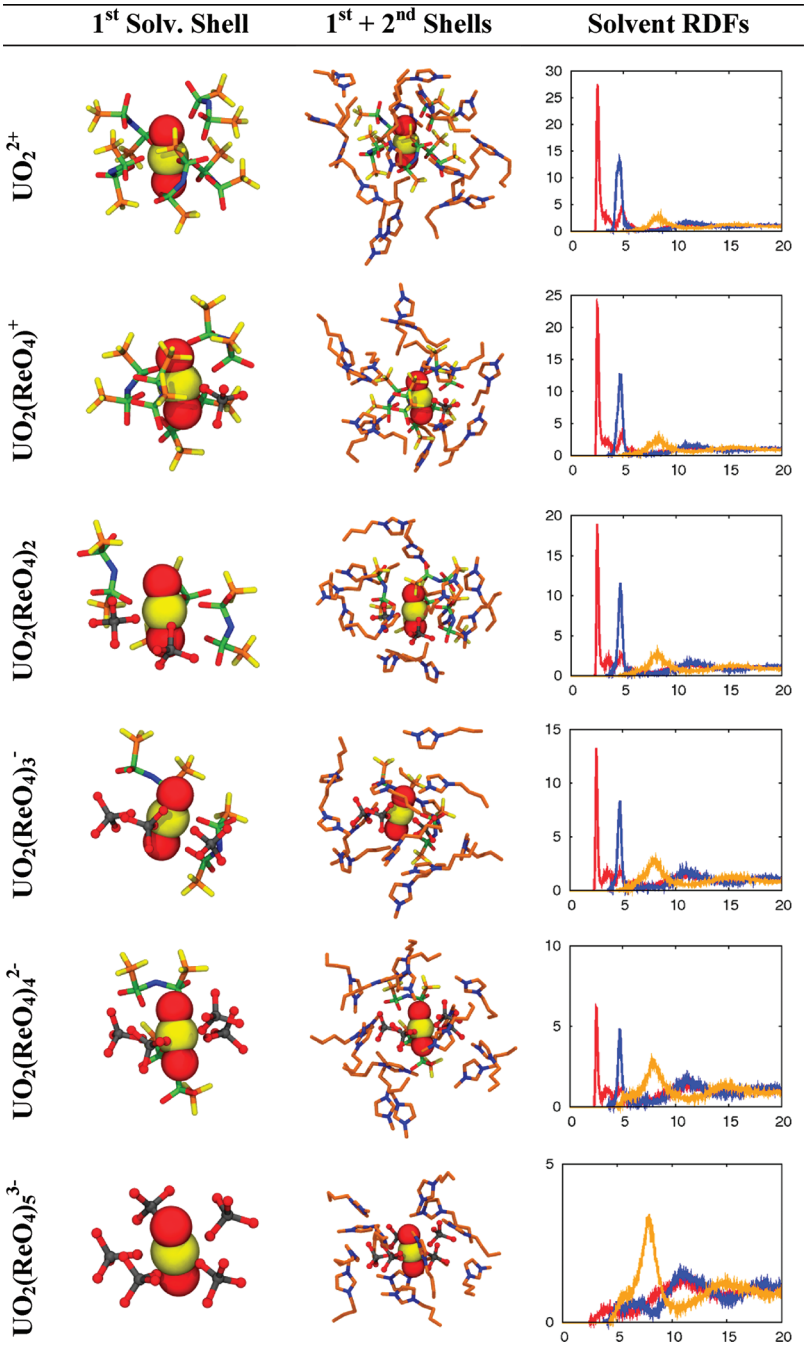

Figure 4. $UO_2(ReO_4)_n^{2-n}$ complexes (n = 0–5) in [Bmi][Tf_2N]: typical snapshots of their 1st and 1st + 2nd solvation shells and solvent O_{Tf2N} (red), N_{Tf2N} (blue), and N_{butyl} (orange) RDFs around UO_2^{2+}. The results for the [$MeBu_3N$][Tf_2N] solution are given in Figure S8, Supporting Information.

decreases to a minimum energy value of −3.7 kcal/mol at 6.5 Å, indicating that the dimer is more stable than these two monomers in the IL solution. The $(UO_2)_2(ReO_4)_8^{4-}$ dimer is similar to the one observed in acetonitrile, with two bridging ReO_4^- anions and 3 exo ReO_4^- ligands on each uranyl cation. It is surrounded by ca. 14 Bmi^+ cations H-bonded via their imidazolium ring protons to the anionic ligands (Figure 6b). Tf_2N^- anions are not directly coordinated to the UO_2^{2+} cations, but some are inserted in the Bmi^+ cationic shell.

UV–VIS AND EXAFS RESULTS

In Water. We first recorded the absorbance of aqueous solutions of UO_2^{2+} at increasing $HReO_4$ concentrations (see Figure 7 for some spectra). The spectrum of UO_2^{2+} in $HClO_4/H_2O$ ([$HClO_4$] = 1 M, R = 0), which has been recorded as a reference, peaks at λ_{max} = 414 nm, in agreement with previous studies indicating a maximum at 413.8 nm with ε in the range of 7–10 M^{-1} cm^{-1} for free uranyl in water.[60,61] For the first $HReO_4$ series (see Experimental section), below [$HReO_4$] = 1 M (R < 100), all recorded spectra look the same and are very similar (if not identical) to that recorded for $HClO_4$, but above this value, a shift is observed in λ_{max}, which is significant at [$HReO_4$] = 1.22 M, corresponding to R = 122. Owing to solubility limits, with uranyl concentrations in the range of 10^{-2} M, as required for UV–vis spectroscopy, it is impossible to reach R ratio above ca. 620.

To go a step further, we then performed TRLFS experiments. With the help of laser excitation, uranyl concentration

dx.doi.org/10.1021/jp209476h | J. Phys. Chem. B 2012, 116, 3205–3219

Table 2. Solvation of $UO_2(ReO_4)_n^{2-n}$ (n = 0−5) in IL; Characteristics of Solvent RDFs around the U Atom; Integration of the First RDF Peak up to the First Minimum; Distances (Å) of the First Maximum and Minimum in Parentheses

	[Bmi][Tf_2N] solution		
	O_{Tf2N}−UO_2^{2+}	N_{Tf2N}−UO_2^{2+}	N_{Bmi}−UO_2^{2+}
UO_2^{2+}, 6 ReO_4^-	5.7 (2.54; 3.04)	5.0 (4.62; 6.40)	13.1 (8.28; 11.76)
$UO_2(ReO_4)^+$, 5 ReO_4^-	4.9 (2.52; 3.22)	4.1 (4.76; 6.24)	11.9 (8.40; 11.00)
$UO_2(ReO_4)_2$, 4 ReO_4^-	3.2 (2.50; 3.00)	3.5 (4.70; 6.50)	12.2 (8.26; 10.92)
$UO_2(ReO_4)_3^-$, 3 ReO_4^-	2.1 (2.52; 3.02)	2.1 (4.76; 5.48)	11.9 (8.06; 10.86)
$UO_2(ReO_4)_4^{2-}$, 2 ReO_4^-	1.1 (2.54; 3.00)	1.5 (4.72; 6.14)	12.8 (8.04; 11.26)
$UO_2(ReO_4)_5^{3-}$, ReO_4^-	[a]	[a]	11.7 (7.94; 10.48)
	[$MeBu_3N$][Tf_2N] solution		
	O_{Tf2N}−UO_2^{2+}	N_{Tf2N}−UO_2^{2+}	N_{MeBu3N}−UO_2^{2+}
UO_2^{2+}, 6 ReO_4^-	6.1 (2.54; 3.12)	4.3 (4.54; 5.56)	10.3 (8.92; 11.76)
$UO_2(ReO_4)^+$, 5 ReO_4^-	5.0 (2.54; 3.20)	4.0 (4.68; 7.66)	10.8 (8.72; 11.92)
$UO_2(ReO_4)_2$, 4 ReO_4^-	3.4 (2.54; 3.10)	3.0 (4.72; 7.54)	9.1 (7.98; 10.96)
$UO_2(ReO_4)_3^-$, 3 ReO_4^-	2.1 (2.52; 3.02)	2.0 (4.76; 5.52)	10.8 (8.2; 12.06)
$UO_2(ReO_4)_4^{2-}$, 2 ReO_4^-	1.0 (2.52; 2.98)	1.0 (4.68; 5.50)	9.5 (7.98; 10.78)
$UO_2(ReO_4)_5^{3-}$, ReO_4^-	[a]	[a]	9.7 (7.74; 10.90)

[a] III-defined first peak.

can be decreased to 10^{-5} M or lower without affecting sensitivity[62−64] so that speciation at the trace level is easily performed in various systems[65−68] by monitoring changes in the fluorescence characteristics of uranyl (lifetime and emission spectra). However, ReO_4^- strongly absorbs in the UV range, thus hampering the direct excitation of uranyl to occur and limiting the maximum value of R we could reach. We thus recorded the fluorescence uranyl parameters in the range $10 < R < 6400$ (Figure 8). Up to $R \leq 1970$, no change in the fluorescence spectra could be observed, and the peak maxima, located at 488/510/534/560 nm, are in very good agreement with the values already published for the free UO_2^{2+} ion.[69] By contrast, for $R > 1970$, shifts in the emission maxima are obvious. For [$HReO_4$] = 3.43 M, the three emission maxima are shifted to 491/512/534 nm, and these values are further increased to 495/520/545 nm at $R \approx 6400$ (see Figure 8).

In Acetonitrile. Figure 9 displays the spectral evolution observed by the addition of increasing amounts of ReO_4^-, from R = 0 to R = 20. Changes are obvious between R = 0, 1, and 2, and the spectral features still evolve as R is increased above 2, reaching, nevertheless, a limiting spectrum. Spectra recorded for R from 3 to 5 are almost identical to each other, and the spectra for R = 10 and 20 are very similar too, except for the appearance of a small peak at 455 nm at these two high R values.

Figure 10 displays the EXAFS and FT spectra obtained at the U L_{III} edge for two samples of uranyl + perrhenate in acetonitrile, at R = 0 and R = 5. Fit results are given in Table 4. For R = 0, the first U neighbors are found at 2.46 Å, on average. EXAFS is not able to distinguish between O and N atoms, due to their close masses. Anyhow, the distance found here is larger than typical U−O_{Tf2N} distances of 2.43 Å[24] but smaller than the U−N_{MeCN} distance of 2.53 Å fitted by Hennig et al.[19] This suggests that the equatorial shell of uranium involves a mixture of acetonitrile and Tf_2N^- ligands (R = 0). The addition of perrhenate ions as $BmiReO_4$ at a ratio R = 5 entails a significant shortening of the U equatorial bonds to 2.37 Å, as a sign of changes in the uranyl coordination sphere. No direct U−Re interaction is evidenced. The same sample was also measured at the Re L_{III} edge (see Figure 11). Here again, no U−Re signal is detected. Rhenium is found to be surrounded by 4 oxygen atoms at 1.74 Å, which is the typical structure of perrhenate units.[70,71]

In ILs. In the range 250−300 nm, the two tetraalkylammonium-based ILs display an absorption peak that is almost absent in [Bmi][Tf_2N] (Figure S9, Supporting Information). By comparison to previous works in imidazolium-based ILs,[69,72] this peak can be ascribed to impurities remaining from the synthesis. Owing to the strong absorption of the ILs, especially in the case of [Bu_3MeN][Tf_2N], UV−vis data below 350 nm were not considered. In a second step, we recorded the UV−vis absorption spectra of ReO_4^- alone (introduced via the $BmiReO_4$, $Me_3BuNReO_4$, or $Bu_3MeNReO_4$ salts) and of UO_2^{2+} alone (introduced via the $UO_2(Tf_2N)_2$ salt) in the three ILs. In all cases, ReO_4^- displays a strong absorption below 300 nm, but differences between the various spectra are not significant because the signal is close to saturation, due to the already strong absorption of the pure ILs. By contrast, the differences observed in the UV−vis absorption spectra of UO_2^{2+} in the range 380−520 nm from one IL solvent to the other (see Figure 12) are significant. The spectrum recorded in [Bmi][Tf_2N] is in agree-

Table 3. Energy Analysis of $UO_2(ReO_4)_n^{2-n}$ Complexes (n = 0−5) in IL; Total Energy of the System (E_{TOT}) and Its Intra Complex (E_{COMP}), Intrasolvent (E_{ILIL}), and Complex−Solvent Interaction (E_{SOLV}) Energy, $E_{TOT} = E_{COMP} + E_{ILIL} + E_{SOLV}$[a]

solute	E_{COMP}	E_{SOLV}	E_{ILIL}	E_{TOT}
	[Bmi][Tf_2N] Solution			
UO_2^{2+}, 6 ReO_4^-	2 ± 2	−564 ± 19	5205 ± 68	4644 ± 66
$UO_2(ReO_4)^+$, 5 ReO_4^-	−178 ± 4	−339 ± 15	5147 ± 63	4631 ± 61
$UO_2(ReO_4)_2$, 4 ReO_4^-	−290 ± 7	−256 ± 17	5165 ± 63	4619 ± 61
$UO_2(ReO_4)_3^-$, 3 ReO_4^-	−372 ± 11	−229 ± 55	5280 ± 62	4679 ± 61
$UO_2(ReO_4)_4^{2-}$, 2 ReO_4^-	−376 ± 9	−357 ± 19	5390 ± 65	4656 ± 64
$UO_2(ReO_4)_5^{3-}$, ReO_4^-	−332 ± 7	−582 ± 20	5545 ± 64	4630 ± 62
	[$MeBu_3N$][Tf_2N] Solution			
UO_2^{2+}, 6 ReO_4^-	2 ± 2	−559 ± 17	7621 ± 74	7065 ± 73
$UO_2(ReO_4)^+$, 5 ReO_4^-	−178 ± 4	−340 ± 15	7593 ± 78	7075 ± 77
$UO_2(ReO_4)_2$, 4 ReO_4^-	−302 ± 12	−221 ± 26	7583 ± 77	7060 ± 75
$UO_2(ReO_4)_3^-$, 3 ReO_4^-	−381 ± 6	−188 ± 12	7659 ± 78	7079 ± 77
$UO_2(ReO_4)_4^{2-}$, 2 ReO_4^-	−381 ± 7	−320 ± 17	7658 ± 75	6956 ± 75
$UO_2(ReO_4)_5^{3-}$, ReO_4^-	−335 ± 8	−541 ± 17	7919 ± 72	7042 ± 70

[a] Note that uncomplexed ReO_4^- anions are considered as part of the IL. Averages are taken over the last 1 ns of the 5 MD runs.

dx.doi.org/10.1021/jp209476h | J. Phys. Chem. B 2012, 116, 3205−3219

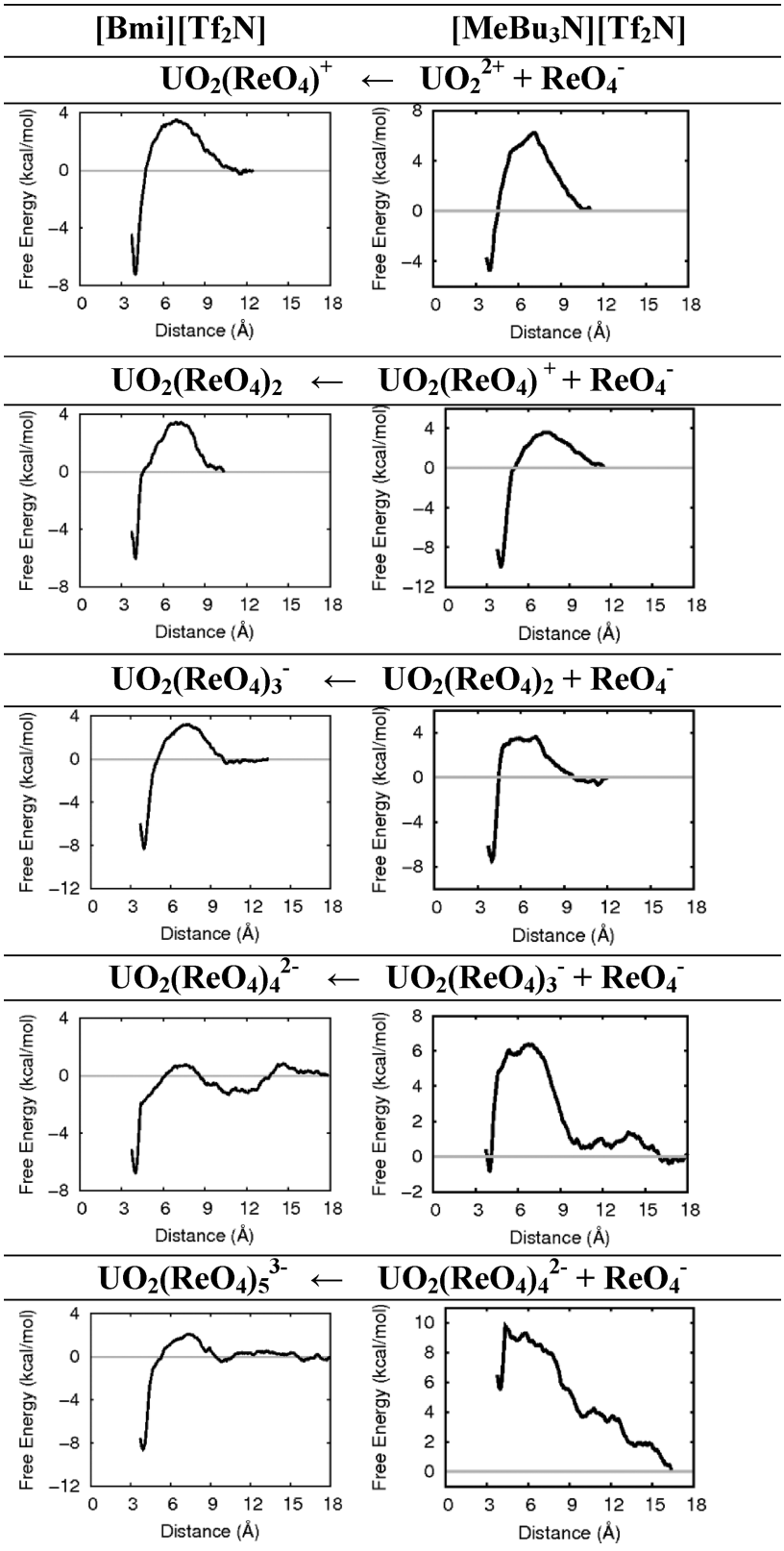

Figure 5. Free energy profiles upon the successive complexation of ReO_4^- to uranyl in $[Bmi][Tf_2N]$ (left) and $[MeBu_3N][Tf_2N]$ (right).

ment with those already published in this IL[73] but differs markedly from those in $[Me_3BuN][Tf_2N]$ and $[Bu_3MeN][Tf_2N]$ that are close to each other. In particular, the maximum observed at 412 nm in $[Me_3BuN][Tf_2N]$ and $[Bu_3MeN][Tf_2N]$ is close to the well-known maximum at 413.8 nm in water[60,61] but is shifted to 420 nm in $[Bmi][Tf_2N]$. In all ILs, the molar absorption coefficient is low, as it is in water. The EXAFS measurements in $[Bu_3MeN][Tf_2N]$ for R = 0 show that the uranium environment is similar to the one already published for $[Bmi][Tf_2N]$,[24] with 5 equatorial oxygen atoms at 2.43 Å.

The addition of increasing amounts of ReO_4^- in $[Bu_3MeN][Tf_2N]$ leads to drastic changes of the uranyl absorption spectra

dx.doi.org/10.1021/jp209476h | J. Phys. Chem. B 2012, 116, 3205−3219

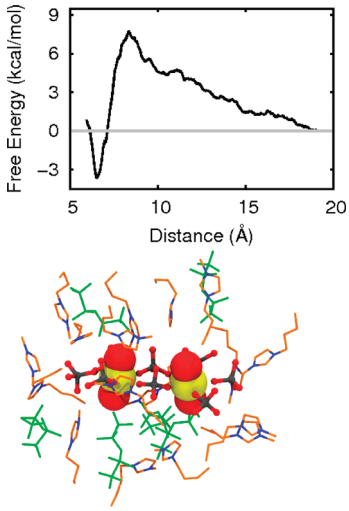

Figure 6. a) Top: calculated free energy change for the formation of the $(UO_2)_2(ReO_4)_8^{4-}$ dimer from two $UO_2(ReO_4)_4^{2-}$ species in [Bmi][Tf_2N], as a function of the U···U distance. Bottom: snapshot of the dimer formed at the free energy minimum.

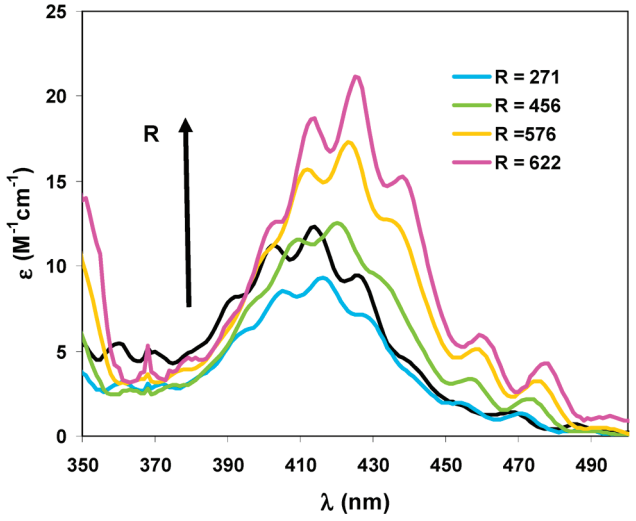

Figure 7. Molar absorption coefficient of uranyl in aqueous solutions as a function of R = Re/U. Black line: [$HClO_4$] = 1 M (see text).

(Figure 13) that are very similar from one IL to the other, thus fading away the differences pointed above for R = 0. The spectral evolution in the three ILs differs from that obtained in acetonitrile. In particular, the small peak at 457 nm is already visible in all three ILs at R = 5, while it becomes visible in acetonitrile only for $R \geq 10$. Furthermore, shoulders appear in the peaks located at 403, 414, 427, and 442 nm in the three IL solvents at R = 10, which are not present in acetonitrile, even at R = 20. EXAFS results for R = 10 indicate, as in acetonitrile, a shortening of the equatorial distances to 2.37 Å and a slight decrease of the equatorial coordination number. Here again, no U−Re interactions are detected.

DISCUSSION

Whatever the solvent (water, acetonitrile, or any of the three ILs), our results, both theoretical and experimental, evidence a complexation process between UO_2^{2+} and ReO_4^- but up to quite different extents, depending on the solvent. From an experimental side, changes observed in the UV−vis uranyl

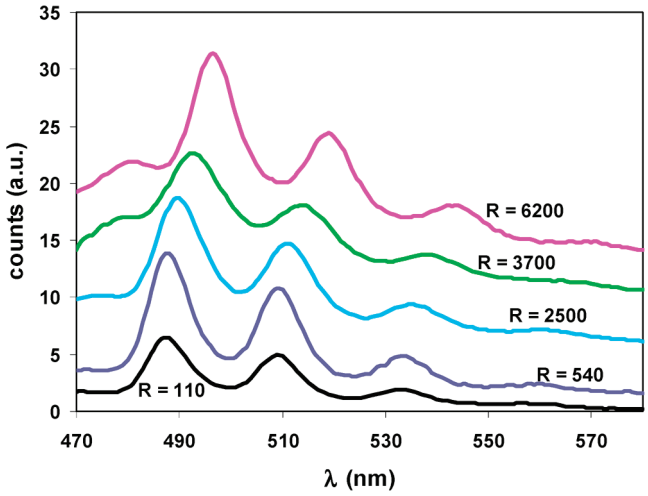

Figure 8. Emission spectra of uranyl in aqueous solutions as a function of R = Re/U. Spectra have been shifted along the y axis.

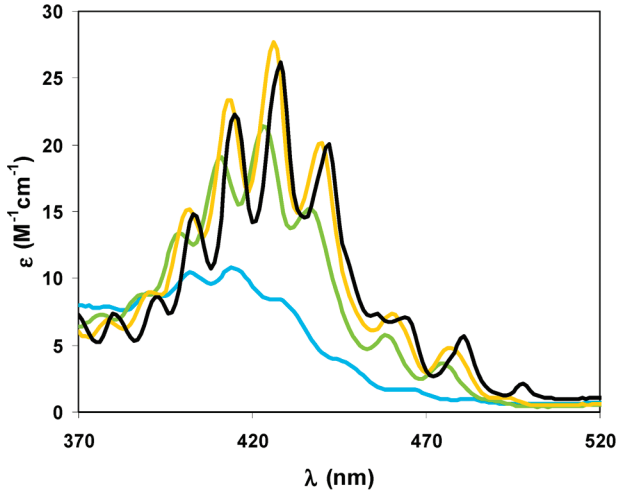

Figure 9. Molar absorption coefficient of uranyl in acetonitrile solutions as a function of R = Re/U. Blue, R = 0; green, R = 1; yellow, R = 2; black, R = 20.

spectra in water (Figure 7), acetonitrile (Figure 9), and the three ILs (Figure 13) are a signature for complexation, as is the change in the emission spectra in water (Figure 8). The reduction in bond distances as observed by EXAFS in acetonitrile and [Bu_3MeN][Tf_2N] is also indicative of complexation (Table 4). However, the R values at which complexation occurs impose to distinguish water on the one hand, and acetonitrile and the three ILs on the other hand, as also indicated by the MD results.

In water, the MD simulations indicate that no dominant $U^{(VI)}/Re^{(VII)}$ complex exists for long periods of time, even for rather high R values in the range 2−125, which is in line with the UV−vis experiments, indicating that complexation occurs for $R \geq 100$. It is, therefore, not possible to derive any complexation constant, as the activity coefficient expressions (through SIT or Pitzer formalism, for example) are not tabulated at any ionic strength for ReO_4^-. Nevertheless, some hints can be derived by comparison with the data in acetonitrile. In fact, the UV−vis spectrum obtained for R = 1 in acetonitrile matches rather well with that obtained for $R \approx 580$ in water. For higher R values in water, the bathochromic shift

dx.doi.org/10.1021/jp209476h | J. Phys. Chem. B 2012, 116, 3205−3219

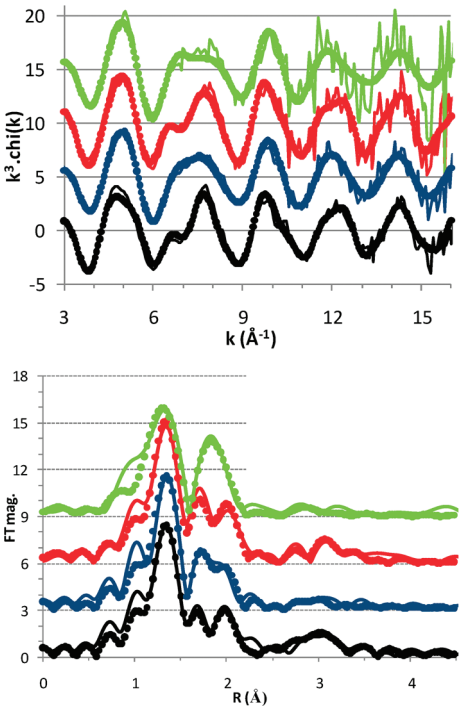

Figure 10. EXAFS spectra and their Fourier transform obtained at the U L_{III} edge. Black: R = 0 in acetonitrile. Blue: R = 5 in acetonitrile. Red: R = 0 in $[Bu_3MeN][Tf_2N]$. Green: R = 10 in $[Bu_3MeN][Tf_2N]$.

observed does not allow to superimpose the spectrum to that at R = 1 in acetonitrile anymore. It is thus reasonable to assume that $UO_2ReO_4^+$ is formed in aqueous solutions in significant amounts for R > 100 and is dominating the speciation at $R \approx$ 580, in line with the average coordination number of 1.1 derived from MD calculations. Turning to the TRLFS results, they do not evidence any spectral changes up to $R \approx$ 1970 as compared to the free UO_2^{2+} emission spectrum; we therefore conclude that the $UO_2ReO_4^+$ species (observed by UV–vis already for R = 100) is very weakly luminescent. This is a rather unusual situation, with few such examples in the literature: in water, Sladkov et al. evidenced a weakly luminescent uranyl complex with SeO_3H^-,[74] and $UO_2(CO_3)_3^{4-}$ has been shown to be nonluminescent.[75,76] By contrast, above R = 1970, the shift in the emission maxima we observe for the aqueous samples are to be ascribed to, at least, one additional luminescent U/Re complex of higher stoichiometry. Although the variation of the peak maxima is the signature of a complexation process, there is no correlation between emission peak values and uranyl stoichiometry. For example, in water, uranyl emission maxima observed for 1:2 complexes greatly vary from one ligand to the other: they peak at 493/514/538 nm for $[UO_2(SO_4)_2]^{2-}$,[68] at 497/518/541 nm for $UO_2[H_2AsO_4]_2$,[65] and at 501/522/545 nm for $UO_2(IO_3)_2$.[77] Again, comparison with the acetonitrile data can give some hints for the possible stoichiometry. The best match with R = 2 in acetonitrile, although not perfect, especially as far as relative intensities of the peaks are concerned, is for R = 622 in water, the highest R value we could examine in our study. This does not prove, however, that the rather similar UV–vis spectra observed in acetonitrile and water for R = 2 and R = 622, respectively, correspond to a unique $UO_2(ReO_4)_2$ species. Unsaturated complexes like $UO_2(ReO_4)_2$ can further coordinate solvent molecules to form, e.g., $UO_2(ReO_4)_2(H_2O)_n$ in water and $UO_2(ReO_4)_2(MeCN)_{)m}$ complexes in acetonitrile. The underlying assumption, that both types of complexes have the same spectroscopic UV–vis signature, remains to be assessed. Considering the rapid exchange between the different labile complexes observed in the MD calculations in water, it is more likely that various complexes are simultaneously present in nonnegligible amounts in these samples. Again, this is in line with the coordination number of 2.1 obtained in the MD calculations, with evidence of zero- and pentacomplexes coexisting in solution.

We now turn to the examination of the results obtained in acetonitrile and in the three ionic liquids, considering first the solutions without added ReO_4^- (R = 0) as a reference. Comparison of the uranyl UV–vis spectra in these four solvents (Figure 12) evidence similarities, in terms of peak positions, between the two ammonium-based ILs and, to a lesser extent, with acetonitrile also, whereas the spectrum in $[Bmi][Tf_2N]$ is quite different. The fact that the two ammonium-based ILs yield similar spectra is not surprising, owing to their close chemical structures. The difference between Bmi^+ and ammonium-based ILs can be explained by the onion-type solvation patterns of metallic cations in ILs[4,24,25,51,78] and the modulation of the anionic first shell composition by the cationic second shell. Indeed, according to the MD simulations in the ILs, uranyl coordinates only Tf_2N^- ligands, forming $UO_2(Tf_2N)_n^{2-n}$ anionic complexes (see snapshots on top of Figures 4 and S8, Supporting Information, and RDF analysis in Table 2). Interestingly, the number of coordinated Tf_2N^- ligands is somewhat higher in the Bmi^+ than in the Bu_3MeN^+-based IL (n = 5.0 and 4.3, respectively), in keeping with the stronger interactions with second shell cations (13.1 Bmi^+ versus 10.3 Bu_3MeN^+ cations; also note the H-bonding features

Table 4. EXAFS Fit Results[a]

	CH_3CN solution		$[Bu_3MeN][Tf_2N]$ solution	
solute	$UO_2(Tf_2N)_2$	$UO_2(Tf_2N)_2$ 10^{-2} M + $BmiReO_4$ 5.10^{-2} M	$UO_2(Tf_2N)_2$	$UO_2(Tf_2N)_2$ 10^{-2} M + $BmiReO_4$ 10^{-1} M
U L_{III} edge	2 O_{ax} @ 1.75(4) Å[b]	2 O_{ax} @ 1.76(1) Å[b]	2 O_{ax} @ 1.76(1) Å[b]	2 O_{ax} @ 1.76(2)Å[b]
	σ^2 = 0.0014(5) Å^2	σ^2 = 0.0016(6) Å^2	σ^2 = 0.001(1) Å^2	σ^2 = 0.0 02(2) Å^2
	5.1(3) N @ 2.46(9) Å	4.2(9) O @ 2.37(2) Å	5.5(1) O @ 2.43(6) Å	4.2(3) O @ 2.37(3) Å
	σ^2 = 0.008(7) Å^2	σ^2 = 0.008(7) Å^2	σ^2 = 0.009 Å^2	σ^2 = 0.005(6) Å^2
	E_0 = −9.5 eV	E_0 = −9.5 eV	E_0 = −7.4 eV	E_0 = −9.5 eV
	R_{factor} = 0.04	R_{factor} = 0.04	R_{factor} = 0.03	R_{factor} = 0.05
Re L_{III} edge		3.6(1) O @ 1.74(1) Å		
		σ^2 = 0.001(8) Å^2		
		E_0 = 2.9 eV		
		R_{factor} = 0.04		

[a] σ^2 is the Debye-Waller factor, E_0 is the threshold energy, R_{factor} is the goodness of the fit.[48] [b] Fixed parameters during the fit.

dx.doi.org/10.1021/jp209476h | J. Phys. Chem. B 2012, 116, 3205–3219

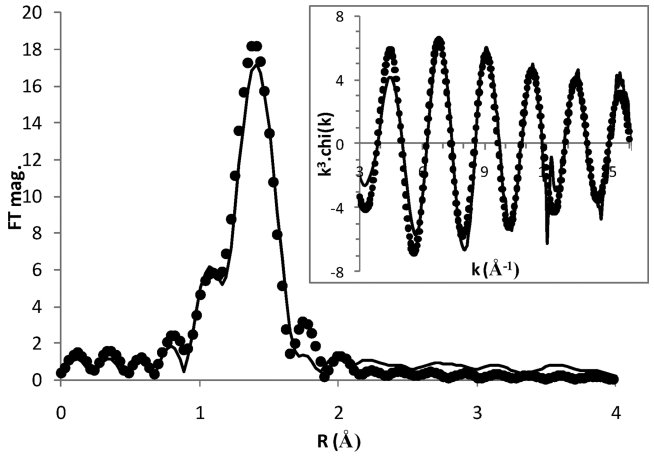

Figure 11. EXAFS spectrum and its Fourier transform obtained at the Re L_{III} edge for the sample R = 5 in acetonitrile.

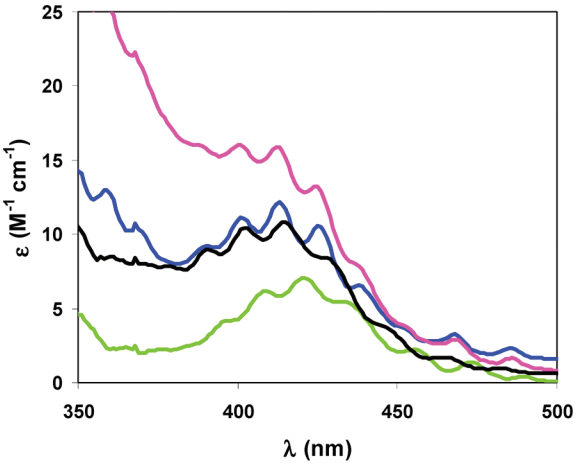

Figure 12. Molar absorption coefficient of uranyl dissolved in the three degassed ILs. Green, [Bmi][Tf_2N]; blue, [Me_3BuN][Tf_2N]; pink, [Bu_3MeN][Tf_2N]; black, CH_3CN.

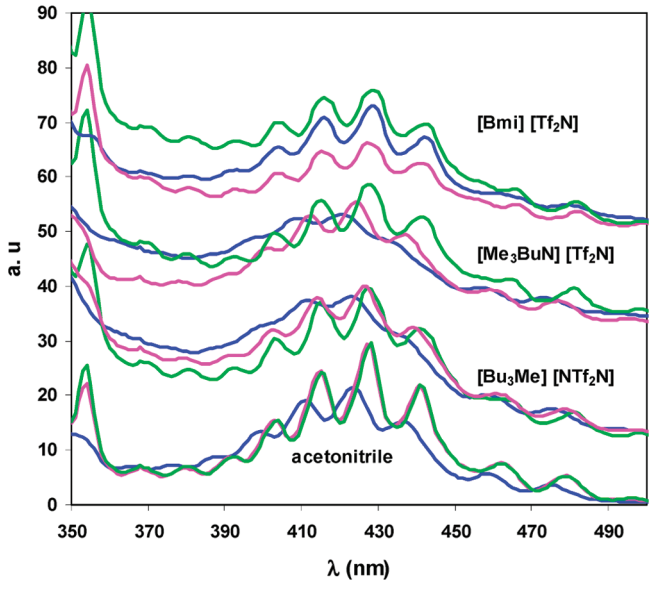

Figure 13. Molar absorption coefficient of uranyl in acetonitrile and the three ILs. Spectra have been shifted along the y axis for clarity. Blue, R = 1; pink, R = 3; green, R = 4.

of Bmi^+ to Tf_2N^- ligands). Differences in the first and second coordination spheres can thus be the rationale for the changes observed in the uranyl UV–vis spectra. In acetonitrile, the most probable species is $UO_2(Tf_2N)_2\cdot(CH_3CN)_m$, as found in the MD simulation where m = 2 and Tf_2N^- ligands adopt different polydentate coordination modes (see Figure S3, Supporting Information, top left). As a result, the similarities between UV–vis spectra in acetonitrile and the tetraalkylammonium ILs would be quite fortuitous.

We now examine the effect of added ReO_4^- in acetonitrile and in the three ILs. Complexation occurs in all four solvents, as evidenced by the changes in the UV–vis spectra (see Figure 13 for some spectra for R = 1, 3, and 4) and EXAFS data (Table 4). For R = 4, the UV–vis spectra in all four solvents are very similar to each other, by contrast to the case R = 0 discussed above. This can be interpreted by the formation of similar dominant complexes where ReO_4^- has displaced Tf_2N^- ligands (plus MeCN ligands in acetonitrile).

In the different solvents, UV–vis spectra do not evolve further above R = 10 to 20, indicating that complexation has reached its limits between R = 10 and 20 or even below values at which ReO_4^- is not complexed at all in water. This shows that competition for the first coordination sphere of uranyl is greatly in favor of ReO_4^- in these four solvents but not in water. A close examination of the various spectra above R = 4 indicates that complexation is only slightly different in acetonitrile as compared to the ILs, hinting for a higher stoichiometry of the uranyl complex in the ILs. In particular, we tentatively ascribe the shoulders at 417, 429, 442, and 446 nm, (see Figure S10, Supporting Information, for spectra in [Bu_3MeN]-[Tf_2N] at different R values) observed in the ILs at the highest R values, to the appearance of $[UO_2(ReO_4)_4]^{2-}$, by comparison to the characteristic band splitting of $UO_2Cl_4^{2-}$ in [Bmi][Tf_2N] and [Bu_3MeN][Tf_2N].[79] In acetonitrile, considering that UV–vis spectra do not evolve much from R = 3 to R = 10, we propose $UO_2(ReO_4)_3^-$ to be the limiting complex obtained in this solvent. Note that a Re/U ratio of 3 would also be consistent with a uranyl dimer of $[(UO_2)_2(ReO_4)_8]^{4-}$ composition, as found in MD simulations. There is, however, no spectroscopic evidence of such a dimer in solution.[80] Generally speaking, to our knowledge, no uranyl dimers in solutions have been assessed so far through UV–vis and EXAFS, preventing any comparison. For example, (i) the uranyl dimers with bridging perrhenates and phosphoryl ligands observed in the solid state could not be characterized in solution,[71] (ii) the dimeric uranyl complex with bridging carboxylic ligands formed in the solid state from a betaine-based IL dissociates upon dissolution in water and in acetonitrile.[81]

On the basis of present and previous publications, we can now attempt to order the complexing abilities toward uranyl in water, acetonitrile, and ILs of this work, of the following X^- ligands: NO_3^-, Cl^-, ReO_4^-, and ClO_4^-.[82] For the discussion to follow, we define a strong X^- ligand as a ligand forming at almost 100% of the $[UO_2(X)_n]^{2-n}$ species at R values equal to n (n = 1 up to the limiting complex). Otherwise, ligands will be called weak ones, and their relative strengths can be tentatively ordered.[83] Under this frame, NO_3^- and Cl^- are weak ligands in water of similar strengths: $UO_2NO_3^+$ is detected for NO_3^-/UO_2^{2+} = 38, and $UO_2(NO_3)_3^-$ is the limiting complex observed at NO_3^-/UO_2^{2+} = 360,[84] while UO_2Cl^+ is observed at Cl^-/UO_2^{2+} = 40, and the limiting species $UO_2(Cl)_3^-$ is evidenced at Cl^-/UO_2^{2+} = 350.[85] For ReO_4^-, much higher values are necessary to evidence $UO_2(ReO_4)^+$ ($R \geq 100$, UV–vis data)

dx.doi.org/10.1021/jp209476h | J. Phys. Chem. B 2012, 116, 3205–3219

and $UO_2(ReO_4)_2$ (R > 1970, TRLFS data), indicating that ReO_4^- behaves as a weaker ligand than NO_3^- or Cl^-. The tetrahedral analogue of perrhenate, ClO_4^-, appears weakest of the examined series, as EXAFS data could not evidence complexation up to ClO_4^-/UO_2^{2+} = 1150.[20,86] In acetonitrile, NO_3^- is a strong ligand, as the limiting complex $[UO_2(NO_3)_3]^-$ dominates the speciation in acetonitrile for $R \geq 3$.[5,87] Similarly, Cl^- readily forms the limiting complex $[UO_2Cl_4]^{2-}$ at R = 4.[19,88] Again, ClO_4^- anions are rather weak ligands in acetonitrile: at R = 2, uncoordinated perchlorate ions amount to 37% and only 1.6 ClO_4^- are coordinated to uranyl on average at R = 5.[89] Thus, in acetonitrile, ReO_4^- should be a slightly weaker ligand than Cl^- and NO_3^- but stronger than ClO_4^-. Finally, in [Bmi][Tf_2N], $[UO_2(NO_3)_3]^-$ is dominating the speciation for $R \geq 3$,[5,87] while in [Bmi][Tf_2N] and [Bu_3MeN][Tf_2N], the 1:4 chloro complex is dominating the speciation already at a ratio Cl^-/UO_2^{2+} = 4.[79] By contrast, ReO_4^-/UO_2^{2+} ratio above 10 are required to reach the same 1:4 stoichiometry. UO_2^{2+}/ClO_4^- data in ILs are too scarce to allow ordering, but uranyl−perchlorate complexation has been evidenced for ClO_4^-/UO_2^{2+} = 2.[4,83] Although incomplete and qualitative, these data suggest that the order of complexing strength found in water ($NO_3^- > Cl^- \gg ReO_4^- \geq ClO_4^-$) pertains in acetonitrile ($NO_3^- \approx Cl^- > ReO_4^- \geq ClO_4^-$) and ILs ($NO_3^- \approx Cl^- > ReO_4^-$). In other words, X^- ligands (even those considered as weak or very weak in water) can behave as strong ones in ILs based on Tf_2N^- anions. In these ILs, differences from one ligand to another are thus attenuated. Acetonitrile appears to be an intermediate case, as ClO_4^- is noncomplexing in water, slightly complexing in acetonitrile, and seems to be rather strong in ILs, but this would deserve additional experimental data to be firmly assessed. Another interesting case would be the triflate anion ($CF_3SO_3^-$) that is considered as noncomplexing in water (like Tf_2N^- and ClO_4^-),[30] while uranyl triflate salts are associated in ILs.[4]

CONCLUSIONS

We report complementary simulation and spectroscopic studies on uranyl complexation with perrhenate anions in different solvents. For this purpose, we synthesized new rhenium salts. Owing to the very weak complexing ability of Tf_2N^- anions, that allows almost any weak ligand to interact with uranyl, ILs thus appear as ideal solvents to study unusual limiting stoichiometries, offering a new playground for structural investigations of metal coordination. Additional experiments would be needed to confirm or to rule out the existence of dimers. As an extension of this work, we expect TcO_4^-, the radioactive homologue of ReO_4^-, to be a rather strong uranyl ligand in ILs, while being a weak uranyl ligand in water. This would be in line with theoretical expectations on the UO_2^{2+}/TcO_4^- binding constant in water.[21] On the basis of the value log β = −0.95 predicted in this publication, and neglecting ionic strength effects, one can calculate that $R = TcO_4^-/UO_2^{2+}$ = 9000 would be needed to observe ca. 50% of the Tc−U complex in water. Experimental and theoretical confirmations of part of these assumptions are under progress in our laboratories and will be the subject of further publications.

ASSOCIATED CONTENT

Supporting Information

IR spectra of the pure degassed ILs. Simulations of different uranyl complexes in acetonitrile. Simulations of $UO_2(ReO_4)_n^{2-n}$ complexes (n = 0−5) in [$MeBu_3N$][Tf_2N]. Simulation results for dimer formation in [Bmi][Tf_2N]. UV−vis. absorption spectra of the three degassed pure ILs and uranyl absorption in acetonitrile and the three ILs. This material is available free of charge via the Internet at http://pubs.acs.org.

AUTHOR INFORMATION

Corresponding Author

*(I.B.) Tel: 33 3 88 10 64 01. Fax: 33 3 88 10 64 31. E-mail: isabelle.billard@iphc.cnrs.fr. (G.W.) Tel: 33 3 68 85 15 44. Fax: 33 3 68 85 16 37. E-mail: wipff@unistra.fr.

Notes

The authors declare no competing financial interest.

ACKNOWLEDGMENTS

This work is financially supported by the French ANR "LILAT". We acknowledge the European Synchrotron Radiation Facility for provision of synchrotron radiation facilities, and we would like to thank Andre Rossberg for assistance in using the ROBL beamline. A.C. and W.G. are grateful to IDRIS, CINES, Université de Strasbourg, and GNR paris for computer resources and to Etienne Engler for assistance.

REFERENCES

(1) Choppin, G. R.; Nash, K. L. *Radiochim. Acta* **1995**, *70/71*, 225.
(2) Mathur, J. N.; Murali, M. S.; Nash, K. L. *Solvent Extr. Ion Exch.* **2001**, *19*, 357.
(3) Ansoborlo, E.; Prat, O.; Moisy, P.; Auwer, C. D.; Guilbaud, P.; Carriere, M.; Gouget, B.; Duffield, G.; Doizi, D.; Vercouter, T.; Moulin, C.; Mouling, V. *Biochimie* **2006**, *88*, 1605.
(4) Gaillard, C.; Chaumont, A.; Billard, I.; Hennig, C.; Ouadi, A.; Wipff, G. *Inorg. Chem.* **2007**, *46*, 4815.
(5) Servaes, K.; Hennig, C.; Billard, I.; Gaillard, C.; Binnemans, K.; Görller-Walrand, C.; Van Deun, R. *Eur. J. Inorg. Chem.* **2007**, 5120.
(6) Georg, S.; Billard, I.; Ouadi, A.; Gaillard, C.; Picquet, M.; Solov'ev, V.; Petitjean, L. *J. Phys. Chem. B* **2010**, *114*, 4276.
(7) Bühl, M.; Sieffert, N.; Chaumont, A.; Wipff, G. *Inorg. Chem.* **2011**, *50*, 299.
(8) Deshayes, L.; Keller, N.; Lance, M.; Navaza, A.; Nierlich, M.; Vigner, J. *Polyhedron* **1994**, *13*, 1725.
(9) Dileep, C. S.; Jagasia, P.; Dhami, P. S.; Achuthan, P. V.; Dakshinamoorthy, A.; Tomar, B. S.; Munshi, S. K.; Dey, P. K. *Desalination* **2008**, *232*, 157.
(10) Mitchell, J. A.; Counce, R. M.; Watson, J. S. *Nucl. Technol.* **2009**, *165*, 360.
(11) Kumari, N.; Pathak, P. N.; Prabhu, D. R.; Manchanda, V. K. *Sep. Sci. Technol.* **2011**, *46*, 79.
(12) Katayev, E. A.; Boev, N. V.; Khrustalev, V. N.; Ustynyuk, Y. A.; Tananaev, I. G.; Sessler, J. L. *J. Org. Chem.* **2007**, *72*, 2886.
(13) Kanellakopulos, B.; Konig, C. P. *Radiochim. Acta* **1983**, *33*, 169.
(14) Macasek, F.; Kadrabova, J. *Radioanal. Chem.* **1979**, *51*, 97.
(15) Lieser, K. H.; Kruger, A.; Singh, R. N. *Radiochim. Acta* **1981**, *28*, 97.
(16) Sutton, A. D.; John, G. H.; Sarsfield, M. J.; Renshaw, J. C.; May, I.; Martin, L. R.; Selvage, A. J.; Collison, D.; Helliwell, M. *Inorg. Chem.* **2004**, *43*, 5480.
(17) Sarsfield, M. J.; Sutton, A. D.; May, I.; John, G. H.; Sharrat, C.; Helliwell, M. *Chem. Commun.* **2004**, 2320.
(18) Nakashima, T.; Lieser, K. H. *Radiochim. Acta* **1985**, 203.
(19) Hennig, C.; Servaes, K.; Nockemann, P.; Hecke, K. V.; Meervelt, L. V.; Wouters, J.; Fluyt, L.; Görller-Walrand, C.; Deun, R. V. *Inorg. Chem.* **2008**, *47*, 2987.
(20) Sémon, L.; Boehme, C.; Billard, I.; Hennig, C.; Lützenkirchen, K.; Reich, T.; Roßberg, A.; Rossini, I.; Wipff, G. *ChemPhysChem* **2001**, *2*, 591.
(21) Buhl, M.; Golubnychly, V. *Inorg. Chem.* **2007**, *46*, 8129.

(22) Billard, I.; Ouadi, A.; Gaillard, C. *Anal. Bioanal. Chem.* **2011**, *400*, 1555.
(23) Sun, X.; Luo, H.; Dai, S. *Chem. Rev.* **2011**, DOI: 10.1021/cr200193x.
(24) Gaillard, C.; Chaumont, A.; Billard, I.; Hennig, C.; Ouadi, A.; Georg, S.; Wipff, G. *Inorg. Chem.* **2010**, *49*, 6484.
(25) Gaillard, C.; Billard, I.; Chaumont, A.; Mekki, S.; Ouadi, A.; Denecke, M.; Moutiers, G.; Wipff, G. *Inorg. Chem.* **2005**, *44*, 8355.
(26) Visser, A. E.; Rogers, R. D. *J. Solid State Chem.* **2003**, *171*, 109.
(27) Dietz, M. L. *Sep. Sci. Technol.* **2006**, *41*, 2047.
(28) Binnemans, K. *Chem. Rev.* **2007**, *107*, 2592.
(29) Billard, I.; Gaillard, C. *Radiochim. Acta* **2009**, *97*, 355.
(30) Gaillard, C.; Azzi, A. E.; Billard, I.; Bolvin, H.; Henning, C. *Inorg. Chem.* **2005**, *44*, 852.
(31) Case, D. A.; Darden, T. A.; Cheatham, T. E., III; Simmerling, C. L.; Wang, J.; Duke, R. E.; Luo, R.; Crowley, M.; Walker, R. C.; Zhang, W.; Merz, K. M.; Wang, B.; Hayik, S.; Roitberg, A.; Seabra, G.; Kolossváry, I.; Wong, K. F.; Paesani, F.; Vanicek, J.; Wu, X.; Brozell, S. R.; Steinbrecher, T.; Gohlke, H.; Yang, L.; Tan, C.; Mongan, J.; Hornak, V.; Cui, G.; Mathews, D. H.; Seetin, M. G.; Sagui, C.; Babin, V.; Kollman, P. A. *AMBER10*; University of California: San Francisco, CA, 2008.
(32) de Andrade, J.; Böes, E. S.; Stassen, H. *J. Phys. Chem. B* **2002**, *106*, 13344.
(33) Canongia-Lopes, J. N.; Padua, A. A. H. *J. Phys. Chem. B* **2004**, *108*, 16893.
(34) Guilbaud, P.; Wipff, G. *J. Mol. Struct.* **1996**, *366*, 55.
(35) Wipff, G.; Schurhammer, R. *J. Phys. Chem. B* **2011**, *115*, 2338.
(36) Sieffert, N.; Wipff, G. *J. Phys. Chem. B* **2006**, *110*, 13076.
(37) Engler, E.; Wipff, G. MD-DRAW Software. Display of Dynamic Structures from MD Simulations. In *Crystallography of Supramolecular Compounds*; Tsoucaris, G., Ed.; Kluwer: Dordrecht, The Netherlands, 1996; p 471.
(38) Humphrey, W.; Dalke, A.; Schulten, K. *J. Mol. Graphics* **1996**, *14*, 33.
(39) Bash, P. A.; Singh, U. C.; Langridge, R.; Kollman, P. A. *Science* **1987**, *236*, 564.
(40) Chipot, C.; Pohorille, A. *Free Energy Calculations. Theory and Appplications in Chemistry and Biology*; Springer: Berlin, Germany, 2007; Vol. *86*.
(41) Frisch, M. J.; Trucks, G. W.; Schlegel, H. B.; Scuseria, G. E.; Robb, M. A.; Cheeseman, J. R.; Montgomery, J. A., Jr.; Vreven, T.; Kudin, K. N.; Burant, J. C.; Millam, J. M.; Iyengar, S. S.; Tomasi, J.; Barone, V.; Mennucci, B.; Cossi, M.; Scalmani, G.; Rega, N.; Petersson, G. A.; Nakatsuji, H.; Hada, M.; Ehara, M.; Toyota, K.; Fukuda, R.; Hasegawa, J.; Ishida, M.; Nakajima, T.; Honda, Y.; Kitao, O.; Nakai, H.; Klene, M.; Li, X.; Knox, J. E.; Hratchian, H. P.; Cross, J. B.; Bakken, V.; Adamo, C.; Jaramillo, J.; Gomperts, R.; Stratmann, R. E.; Yazyev, O.; Austin, A. J.; Cammi, R.; Pomelli, C.; Ochterski, J. W.; Ayala, P. Y.; Morokuma, K.; Voth, G. A.; Salvador, P.; Dannenberg, J. J.; Zakrzewski, V. G.; Dapprich, S.; Daniels, A. D.; Strain, M. C.; Farkas, O.; Malick, D. K.; Rabuck, A. D.; Raghavachari, K.; Foresman, J. B.; Ortiz, J. V.; Cui, Q.; Baboul, A. G.; Clifford, S.; Cioslowski, J.; Stefanov, B. B.; Liu, G.; Liashenko, A.; Piskorz, P.; Komaromi, I.; Martin, R. L.; Fox, D. J.; Keith, T.; Al-Laham, M. A.; Peng, C. Y.; Nanayakkara, A.; Challacombe, M.; Gill, P. M. W.; Johnson, B.; Chen, W.; Wong, M. W.; Gonzalez, C.; Pople, J. A. *Gaussian 03*, revision B.05; Gaussian, Inc.: Wallingford, CT, 2003.
(42) This small-core ECP has been shown to reproduce all-electron scalar relativistic results very well, see: Odoh, S. O.; Schreckenbach, G. *J. Phys. Chem. A* **2010**, *114*, 1957−1963.
(43) Kendall, R. A.; Dunning, T. H. J.; Harrison, R. A. *J. Chem. Phys.* **1992**, *96*, 6769.
(44) Stumpf, S.; Billard, I.; Gaillard, C.; Panak, P.; Dardenne, K. *Radiochim. Acta* **2008**, *96*, 1.
(45) Billard, I.; Georg, S. *Helv. Chim. Acta* **2009**, *92*, 2227.
(46) Tran, C. D.; De Paoli Lacerda, S. H.; Oliveira, D. *Appl. Spectrosc.* **2003**, *57*, 152.
(47) Newville, M. *J. Synchrotron Rad.* **2001**, *8*, 322.
(48) Newville, M.; Ravel, B.; Haskel, D.; Rehr, J. J.; Stern, A.; Yacoby, Y. *Phys. B* **1995**, *208−209*, 154.
(49) Ankudinov, A.; Rehr, J. J. *Phys. Rev. B* **2000**, *62*, 2437.
(50) Chaumont, A.; Wipff, G. *Inorg. Chem.* **2004**, *43*, 5891.
(51) Chaumont, A.; Wipff, G. *Inorg. Chem.* **2009**, *48*, 4277.
(52) On the computational side, note that this feature is well reproduced by the simple FF approach (Table 1) where complexation is mainly described by Coulombic + steric components.
(53) In the neutral $UO_2(ReO_4)_2$ and $UO_2(Tf_2N)_2$ complexes, the two ligands are bidentate, at U−O distances of 2.38 and 2.40 Å, respectively. Tf_2N ligands form 6-membered ring chelates, while ReO_4 forms 4-membered rings that are generally less stable.
(54) Chaumont, A.; Engler, E.; Wipff, G. *Inorg. Chem.* **2003**, *42*, 5348.
(55) Chaumont, A.; Wipff, G. *Phys. Chem. Chem. Phys.* **2003**, *5*, 3481.
(56) Chaumont, A.; Wipff, G. *J. Phys. Chem B* **2004**, *108*, 3311.
(57) Note that this differs from the gas phase (QM results) where $UO_2(ReO_4)_4^{2-}$ should lose one ReO_4^- ligand. In fact, in solution, the U−O_{ReO4} distances are somewhat longer than in the gas phase, thereby reducing the interligand repulsions and favoring a higher coordination number.
(58) Born, M. *Zeit. Phys.* **1920**, *1*, 45.
(59) John, G. H.; May, I.; Sarsfield, M. J.; Collison, D.; Helliwell, M. *Dalton Trans.* **2007**, *16*, 1603.
(60) Karbowiak, M.; Fourest, B.; Hubert, S.; Moulin, C. *Radiochim. Acta* **2003**, *91*, 505.
(61) Meinrath, G.; Kato, Y.; Kimura, T.; Yoshida, Z. *Radiochim. Acta* **1998**, *82*, 115.
(62) Moulin, C.; Charron, N.; Plancque, G.; Virelizier, H. *Appl. Spectrosc.* **2000**, *54*, 843.
(63) Couston, L.; Pouyat, D.; Moulin, C.; Decambox, P. *Appl. Spectrosc.* **1995**, *49*, 349.
(64) Berthoud, T.; Decambox, P.; Kirsch, B.; Mauchien, P.; Moulin, C. *Anal. Chem.* **1988**, *60*, 1296.
(65) Rutsch, M.; Geipel, G.; Brendler, V.; Bernhard, G.; Nitsche, H. *Radiochim. Acta* **1999**, *86*, 135.
(66) Moll, H.; Geipel, G.; Brendler, V.; Bernhard, G.; Nitsche, H. *J. Alloys Compd.* **1998**, *271/273*, 765.
(67) Scapolan, S.; Ansoborlo, E.; Moulin, C.; Madic, C. *J. Alloys Compd.* **1998**, *271/273*, 106.
(68) Bernhard, G.; Geipel, G.; Brendler, V.; Nitsche, H. *Radiochim. Acta* **1996**, *74*, 87.
(69) Billard, I.; Ansoborlo, E.; Apperson, K.; Arpigny, S.; Azehna, A. E.; Birch, D.; Bros, P.; Burrows, H.; Choppin, G. R.; Couston, L.; Dubois, V.; Fanghänel, T.; Geipel, G.; Hubert, S.; Kim, J. I.; Kimura, T.; Klenze, R.; Kronenberg, A.; Kumke, M.; Lagarde, G.; Lamarque, G.; Lis, S.; Madic, C.; Meinrath, G.; Moulin, C.; Nagaishi, R.; Parker, D.; Plancque, G.; Scherbaum, F.; Simoni, E.; Sinkov, S.; Viallesoubranne, C. *Appl. Spectrosc.* **2003**, *57*, 1027.
(70) Katayev, E. A.; Kolesnikov, G. V.; Sessler, J. L. *Chem. Soc. Rev.* **2009**, *38*, 1572.
(71) John, G. H.; May, I.; Sarsfield, M. J.; Collison, D.; Helliwell, M. *Dalton Trans.* **2007**, 1603.
(72) Paul, A.; Mandal, P. K.; Samanta, A. *Chem. Phys. Lett.* **2005**, *402*, 375.
(73) Nockemann, P.; Servaes, K.; Van Deun, R.; Van Hecke, K.; Van Meervelt, L.; Binnemans, K.; Görller-Walrand, C. *Inorg. Chem.* **2007**, *46*, 11335.
(74) Sladkov, V.; Fourest, B.; Mercier, F. *Dalton Trans.* **2009**, 7734.
(75) Saini, R. D.; Bhattacharyya, P. K.; Iyer, R. M. *J. Photochem. Photobiol., A* **1989**, *47*, 65.
(76) Bernhard, G.; Geipel, G.; Reich, T.; Brendler, V.; Amayri, S.; Nitsche, H. *Radiochim. Acta* **2001**, *89*, 511.
(77) Karbowiak, M.; Hubert, S.; Fourest, B.; Moulin, C. *Radiochim. Acta* **2004**, *92*, 489.
(78) Chaumont, A.; Wipff, G. *Chem.—Eur. J.* **2004**, *10*, 3919.
(79) Sornein, M. O.; Cannes, C.; Le Naour, C.; Lagarde, G.; Simoni, E.; Berthet, J. C. *Inorg. Chem.* **2006**, *45*, 10419.

(80) Note that this 1:3 complex has a lower stoichiometry than the one (1:5) observed in MD simulations. The latter can not pretend to yield quantitative results because of force field limitations in classical MD. Furthermore, note the higher simulated concentrations, compared to those experimentally studied. Likewise, the dimers evidenced through MD simulations may not form in our samples owing to the rather low uranyl concentration.
(81) Nockemann, P.; Van Deum, R.; Thijs, B.; Huys, D.; Vanecht, E.; Van Ecke, K.; Meervelt, L.; Binnemans, K. *Inorg. Chem.* **2010**, *49*, 3351.
(82) According to QM calculations in the gas phase, the ClO_4^-, ReO_4^-, and TcO_4^- anions display similar affinities towards the UO_2^{2+} cations and are much weaker ligands than NO_3^-; see Table S4, Supporting Information.
(83) A quantitative comparison requires determination of complexation constants and related thermodynamics data. Such data are unavailable in ILs.
(84) Ikeda-Ohno, A.; Hennig, C.; Tsushima, S.; Scheinost, A. C.; Bernhard, G.; Yaita, T. *Inorg. Chem.* **2009**, *48*, 7201.
(85) Allen, P. G.; Bucher, J. J.; Shuh, D. K.; Edelstein, N. M.; Reich, T. *Inorg. Chem.* **1997**, *36*, 4676.
(86) The uranyl fluorescence lifetime increases upon the addition of $HClO_4$ in water, but this feature has been ascribed to a change in the hydration number of uranyl, without the inner sphere complexation of ClO_4^-.
(87) Ikeda, A.; Hennig, C.; Rossberg, A.; Tsushima, S.; Scheinost, A. C.; Bernhard, G. *Anal. Chem.* **2008**, *80*, 1102.
(88) Servaes, K.; Hennig, C.; Van Deun, R.; Görller-Walrand, C. *Inorg. Chem.* **2005**, *44*, 7705.
(89) Bünzli, J. C. G.; Metabanzoulou, J. P. *Helv. Chim. Acta* **1994**, *77*, 140.